arXiv:astro-ph/9905280v1 21 May 1999

The Role of Stellar Feedback and Dark Matter in the Evolution of Dwarf Galaxies

Andrea Ferrara[1] & Eline Tolstoy[2]

[1]Osservatorio Astrofisico di Arcetri

50125 Firenze, Italy

E–mail: ferrara@arcetri.astro.it

[2]European Southern Observatory

D-85748 Garching bei München, Germany

E–mail: etolstoy@eso.org

Received _____; accepted _____

ABSTRACT

Supernova and multiple supernova events regulate several structural properties of dwarf galaxies. In particular, they govern the metal enrichment and the energy budget of the ISM; they might induce partial (blowout) or total (blowaway) gas removal from the galaxy; they also regulate the pressure of the ISM and consequently the morphology of the galactic gaseous body. Significant amounts of dark matter may play an equally important role: the dark matter gravitational potential tends to concentrate baryons towards the center, thus enhancing both the star formation rate and metal production. Also, the dynamical properties of the ISM, and the occurrence of a blowout or blowaway are shown to be determined by the dark matter content. We present detailed analytical/numerical models describing the evolution of dwarf Irregular galaxies including the above and other effects. The main results are: *(i)* dwarfs with total masses $M \lesssim 5 \times 10^6\ M_\odot$ are blown away; those with gas masses up to $\simeq 10^9\ M_\odot$ lose mass in an outflow; *(ii)* metallicities are found to correlate tightly with dark matter content and are consistent with a range of dark-to-visible mass ratios $\phi \approx 0 - 30$ with about 65% of the dwarfs in the sample having $\phi \approx 0 - 10$; *(iii)* we predict a lower limit to the oxygen abundance in dIs of $12 + log(O/H) \approx 7.2$; *(iv)* outflows are not particularly important for the metallicity evolution of dwarf galaxies and certainly less than star formation for gas consumption; however, dwarfs with gas masses few $\times 10^8\ M_\odot$ are shown to be the major pollutants of the IGM; *(v)* the ISM HI velocity dispersion correlates with metallicity and, indepentently of dark matter, scales as $Z^{3.5}$. Specific comparisons with well studied dI galaxies, as for example Leo A, yield excellent agreement with the data. Based on our results, we discuss a scenario in which late type and early type dwarfs had common progenitors in the past, but differences in their total mass forced these objects to follow different evolutionary paths. Therefore, we consider dI $\rightarrow$ dE transitions occurring at present cosmic times as very unlikely.

Subject headings: galaxies: evolution - dark matter – ISM: abundances - general

1. Introduction

Nearby dwarf galaxies are classified in four basic types: *(i)* Dwarf Irregular (dI) galaxies are the most common type by number, and are usually unstructured gas rich systems with varying levels of star formation occurring in a haphazard manner across the galaxy. The velocity field of the HI gas in these systems is dominated by random motions rather than rotation (Binney & de Vaucouleurs 1981; Staveley-Smith, Davies & Kinman 1992; Lo, Sargent & Young 1993), with peak column densities (as high as $4 \times 10^{21}\mathrm{cm}^{-2}$ or 12 $M_\odot$ pc^{-2}) similar to those of larger galaxies; *(ii)* Blue Compact Dwarf (BCD) galaxies are gas rich systems dominated by very active star formation, and resembling massive HII regions seen in large galaxies. They are thought to be forming stars at a rate which they can only maintain for a short period (Papaderos *et al.* 1994); *(iii)* Dwarf Spheroidal (dSph) galaxies usually have no gas in their center down to very low limits (Knapp *et al.* 1978), although it has been suggested that the gas supply may reside outside the central regions, driven there by supernova explosions and stellar outflows (Puche *et al.* 1992, Carignan 1998; Bowen *et al.* 1997). The stellar distribution of dSph is similar to that of globular clusters, although less centrally concentrated, but a detailed study of the stellar population often reveals that several distinct bursts of star formation have occurred in the past (e.g. Smecker-Hane *et al.* 1994). Finally, *(iv)* Dwarf Elliptical (dE) galaxies look similar to their namesake elliptical galaxies. It was previously thought that they contain only old stars, but new data suggest a sequence of several bursts of star formation, some of which may be quite recent, are needed to explain the characteristics of their stellar population (Ferguson & Binngeli 1994, Babul & Ferguson 1996, Han *et al.* 1997).

Thus, broadly speaking, there are two classes of dwarf galaxies. Late-type (dI and BCD) are star forming systems; the main difference between dI and BCD galaxies seems to be found in their star formation rate - and there is strong evidence that these are otherwise very similar systems (e.g Tolstoy 1998a; Taylor 1997). The other class consists of early-type systems (dSph and dE) which are typically not *currently* forming stars. The difference between dSphs and dEs is not well defined, and lies only in the total mass of the system (dEs are typically more massive than dSphs).

Connecting the above classes of dwarfs in a unified evolutionary scenario has been the subject of considerable study. In fact, in spite of the qualitative differences among the various types, a structural kinship of early and late type dwarfs becomes evident at a more quantitative level. Binggeli (1994) compared the two classes in terms of their central surface brightness and disk scale length vs. absolute blue magnitude for a Virgo cluster sample. He found that early and late types show essentially the same

distribution in such a parameter space. Even before these results, the concept of a transition of some kind from late to early types has been the rationale for a number of studies suggesting different evolutionary schemes. Einasto *et al.* (1974), and later on Lin & Faber (1983), pointed out that since early type dwarfs are often found as satellites of large galaxies, ram pressure stripping in such a high density environment could provide an efficient mechanism to remove all the gas from a galaxy, although Binggeli (1994) gives a list of arguments against it. The importance of the environment for the evolution of galaxies has already been emphasized by Lacey & Silk (1991). The major difficulty is to explain the much lower surface brightness of dIs with respect to dEs. One scenario for the dI $\rightarrow$ dE transition was proposed by Davies & Phillips (1988), who postulated that the gas, instead of being swept away by some transport mechanism, could have been consumed by astration. As it will become clear from our results, astration (as well as outflows) do not appear to be able to rid a galaxy of its ISM. An alternate hypothesis is that dIs and dEs might have had common progenitors, but have evolved differently. What are the reasons for such a behavior ? At least two possibilities need to be considered: *(i)* a difference in the dark matter (DM) content; *(ii)* the effects of the environment. As we will show in this paper the DM fraction must strongly affects the evolution of a low mass galaxy and its star formation history.

Given that the major differences between the two classes reside in their star formation histories, it is important to determine the effects of star formation on the ISM. Among these effects, the most important one is very likely the energy injection from massive stars. Since dwarfs have shallow potential wells, the energy deposition can have consequences that are dramatic in comparison to normal galaxies. Several recent studies of the kinematics of the HI gas in nearby galaxies (e.g. Puche & Westphal 1993, Young & Lo 1996, Hunter et al. 1998, Wilcots & Miller 1998, Van Zee, Skillman & Salzer 1998) show clear evidence of a disturbed ISM, where low density regions, often surrounded by denser shells, expanding at velocities of the order of 15 km s^{-1} are identified. The most natural interpretation of these data implies that these are regions of mechanical energy injection due to stellar (winds and/or SNe) activity. The HI data can even be interpreted as a hint that the least massive galaxies can lose their gas, in a process that we will refer to in this paper as blowaway. Indirect evidence that such a phenomenon might indeed occur is given by Suntzeff *et al.* (1993). By studying the metallicity distribution of stars in the Sextans dwarf galaxy, these authors find that a possible explanation of the observed sharp cut-off at high metallicity is an an almost closed-box evolution followed by a quick removal of gas, or, in our terminology, a blowaway.

If the gas is blown away from the galaxy, one might still expect to find it in the surroundings of dSphs. There is currently no unambiguous evidence for this (e.g. Bowen *et al.* 1997), although there are

tantalising suggestions, (e.g. Carignan *et al.* . 1998), but the limits on diffuse, extended and/or hot gas are not very stringent. ASCA observations (Della Ceca *et al.* 1996; see also Heckman *et al.* 1995) of the star-forming dwarf galaxy NGC1569 have been able to assess the presence of diffuse hot gas ($T \sim 0.7$ keV) very likely heated by supernova explosions. Similarly, Bomans, Chu & Hopp (1997) found X-ray emission from hot gas within a supergiant shell in the dwarf irregular NGC 4449, which also has a large-scale radio synchrotron halo (Klein *et al.* 1996). If the gas remains bound to the galaxy rather than being expelled into the intergalactic medium, after a cooling time it can rain back again onto the galaxy and become available to refuel subsequent star formation, in a process reminiscent of the "galactic fountain" thought to be at work in larger spirals such as the Milky Way. This circulation could in principle provide an attractive explanation for the intermittent star formation activity in dSphs, such as Carina (Smecker-Hane *et al.* 1994) which shows at least four distinct main sequence turn-offs separated by a few Gyr. The difficulty with this scenario is that the required residence time of the gas in the halo seems to be larger than its typical cooling time, unless its density is very low, which is not completely implausible. There are also liable to significant, difficult to quantify, effects from nearby large galaxies.

If energy injection is mainly regulated by massive stars, then the observed metallicity range of dwarfs must be consistent with what is inferred from massive star energetics and dust-to-gas ratio. Several studies (Matteucci & Tosi 1985, Clayton & Pantelaki 1993, Marconi *et al.* 1994; Lisenfeld & Ferrara 1998) have already addressed this issue, and a consensus has been reached that all dwarf galaxies must have lost varying amounts of gas and metals in the past, and probably that they continue to do so today. Metal enhanced outflows can explain the lack of prominent nuclei and the lower-than-average metallicity of low mass systems (Larson 1974), and seem to explain the luminosity-metallicity relationship for dIs (Lequeux *et al.* 1979). The selective loss of metals, particularly oxygen, would also resolve the discrepancy between the yields calculated from stellar evolution theory and those measured by observations (Pagel *et al.* 1992; Maeder 1992). Dekel & Silk (1986) concluded that in order to reproduce the surface brightness and metallicity decline towards low masses, a significant gas loss in a dominant DM halo potential has to take place, with an upper critical halo circular velocity of ~ 100 km s^{-1}. Vader (1986, 1987) put the idea of "metal enhanced" winds on a more quantitative basis. Recent numerical experiments (MacLow & Ferrara 1999, hereafter MF) have shown that indeed during multi-supernova events in dwarf galaxies, most of the metals mixed with the hot cavity gas are able to leave the galaxy, whereas the fraction of cool ISM gas lost is relatively small (at most $\sim$7% of the galaxy mass). Nevertheless, if mixing of the two components in the wind, or with the hot, shell-evaporated interior takes place, this amount of gas is sufficient to dilute the

wind metallicity to a level comparable or only slightly higher than the one of the ISM of the parent galaxy. We will discuss this point in more detail in the section 2.1.1.

Dark matter is the second important ingredient necessary to properly understand dwarf galaxy evolution. Data on the DM content of low mass galaxies, although slowly accumulating are still scarce, and often difficult to interpret. The M/L ratios have been shown to vary between 5.7 and 94 (e.g. Mateo *et al.* 1993, Pryor 1996), confirming the perception that small objects tend to be dark matter dominated. The same conclusion can be reached from rotation curve studies: although exploring the mass distribution only down to relatively large values, a clear trend of increasing dark-to-visible mass ratios with decreasing mass is seen (Mateo 1993).

In this study we consider the effects of stellar feedback and DM on the evolution of dwarfs from a new perspective. There have been a few attempts to combine chemical and dynamical evolution models for dwarf galaxies of various types (Koeppen *et al.* 1995; De Young & Heckman 1994; De Young & Gallagher 1990; Burkert, Theis & Hensler 1993; Silk 1997). Our approach follows naturally from the evidence that supernovae (SNe) and superbubbles (SBs) are the main contributors to the ISM energy budget. Metals are injected into the ISM during every SN explosion event, and if an outflow develops, it allows gas to escape from the disk and even from the gravitational potential of the DM halo. The amount of gas and metals lost is regulated by the pressure in the ISM, which in turn depends upon the energy injection by previous SNe. The pressure is increased as the result of the fact that gas random motions induced by SN explosions generate a non-thermal (turbulent) pressure in addition to the thermal one. Ultimately the pressure can be increased up to the point at which bubbles produced by SNe are confined in the main body of the galaxy, thus inhibiting the outflow. Depressurisation occurs as the parcels of gas (clouds) move and collide at supersonic velocities with respect to their internal sound speed; radiative dissipation behind shocks following collisions then stabilizes the system. On this basis, we expect a correlation between overall dynamical properties, such as gas velocity dispersion, and metallicity of the galaxy.

Very few detailed observations of the velocity dispersion of HI gas in dIs have been made; the situation is made worse by the lack of abundance measurements for those galaxies for which velocity information is available. Only for a handful of galaxies velocity dispersion and metallicity are simulatneously available and so no correlation has yet been firmly established. However, some studies (Lequeux *et al.* 1979; Hunter *et al.* 1982; Matteucci & Chiosi 1983; Skillman, Kennicutt & Hodge 1989) suggest a general trend of increasing metallicity with dynamical mass.

The main aim of this paper is to include the above physical processes, governed by stellar feedback and DM , in a consistent evolutionary model of dwarf galaxies able to explain their most fundamental properties.

The plan of the paper is as follows. In Sec. 2 we present the basic assumptions and equations of our model; Sec. 3 is devoted to simple, but nevertheless physically significant, analytical insights. Sec. 4 discusses the available observations and the dI galaxy sample to which we compare our results. In Sec. 5 we present the results and in Sec. 6 we discuss them along with a possible evolutionary scenario. A brief summary of the results in Sec. 7 concludes the paper.

2. Basic Equations

The equations describing the rate of change of *(i)* the galactic gas mass, M_g; *(ii)* the mass fraction of a given heavy element i, denoted by $X_i = M_i/M_g$ (M_i is the mass of the element i); *(iii)* the kinetic energy stored in ISM bulk motions, $\epsilon_k = \rho\sigma^2$, where ρ is the average ISM density and σ its turbulent velocity dispersion, can be written as

$$\frac{d}{dt}M_g(t) = -\psi(t) + E(t) + A(t) - W(t), \tag{1}$$

$$\frac{d}{dt}[X_i(t)M_g(t)] = -X_i(t)[\psi(t) + W(t)] + E_i(t) + X_{inf}A(t), \tag{2}$$

$$\frac{d}{dt}[\rho\sigma^2(t)] = \dot{\epsilon}(t)^+ - \dot{\epsilon}(t)^-. \tag{3}$$

We will devote each of the following three subsections to the detailed discussion of the various terms appearing in eqs. 1-3. Before doing that, though, it is necessary to describe our galaxy model.

For our purposes, we model a dwarf galaxy as a system initially made of a visible disk with combined gaseous and stellar mass M_g, and a DM halo of mass M_h. We assume that the gas has a density distribution given by $\rho(\varpi, z, \phi) = \rho_0 f(\varpi, z)$, where $\rho_0 = \rho(0, 0)$, ϖ is the galactocentric radius, z is the vertical coordinate, and $f(\varpi, z)$ is a function to be determined, for example, by imposing hydrostatic equilibrium of the gas in the total gravitational potential of the dwarf galaxy, $\Phi_t(\varpi, z) = \Phi_h(\varpi, z) + \Phi_d(\varpi, z)$, as due to the halo and disk components.

The behavior of the dark-to-visible mass ratio $\phi = M_h/M_g$ in galaxies has been explored in great detail in a key study by Persic *et al.* (1996, PSS). These authors find that ϕ is a function of the galactic mass;

using their relations one can derive the dependence of this ratio on the visible mass of the galaxy:

$$\phi \simeq 34.7 M_{g,7}^{-0.29}. \tag{4}$$

where $M_{g,7} = M_g/10^7\ M_\odot$. From this equation it is clear that the gravitational potential of dwarf galaxies with $M_g \lesssim 10^9 M_\odot$ is dominated by the DM halo; therefore we can neglect the potential due to visible mass Φ_d. In the rest of the paper we will not make any specific assumption on ϕ, apart from specific examples where we will use eq. 4.

The density profiles of dwarf DM halos remain uncertain. A comparison between CDM cosmological model predictions and the available observational data, discussed by MF, shows that a considerable disagreement still exist. In view of these uncertainties, we calculate the halo gravitational potential by assuming that the density distribution of the halo can be approximated by a modified isothermal sphere (Binney & Tremaine 1987), which is general enough to be appropriate for an idealized situation such as the one presented here, and does reproduce the observed central core. It follows that

$$\rho_h(r) = \frac{\rho_c}{1 + (r/r_0)^2}. \tag{5}$$

The halo mass as a function of radius is then

$$M_h = M_h(r_h) \simeq 4\pi \rho_c r_0^2 r_h, \tag{6}$$

where r_h is an appropriately defined halo radius. Following a common *Ansatz* we take

$$r_h \equiv r_{200} = \left(\frac{3\rho_c}{200\rho_{crit}}\right)^{1/2} r_0, \tag{7}$$

where r_{200} is the characteristic radius within which the mean DM density is 200 times the present critical density, $\rho_{crit} = 3H_0^2\Omega/8\pi G = 1.88 \times 10^{-29} h^{-2}$ g cm^{-3}, where $H_0 = 100h$ km s^{-1} Mpc^{-1} is the Hubble constant; throughout the paper we will use $\Omega = 1$ and $h = 0.5$. To proceed further we need a relation between the scale radius, r_0, the central DM density ρ_c, and the mass of the halo M_h. Burkert (1995) has shown that the total DM inside r_0, given by $M_0 = M_h(r_0) = \pi(4-\pi)\rho_c r_0^3$, is related to r_0 and ρ_c through the relations

$$M_0 = 7.2 \times 10^7 \left(\frac{r_0}{\mathrm{kpc}}\right)^{7/3} M_\odot, \qquad \rho_c = 2.7 \times 10^7 \left(\frac{r_0}{\mathrm{kpc}}\right)^{-2/3} M_\odot\ \mathrm{kpc}^{-3}. \tag{8}$$

Substituting M_0 and r_h from eq. 7 into equations (8) we get

$$r_0 = 5.3 \times 10^{-5} \left(\frac{M_h}{M_\odot}\right)^{1/2} h^{1/2}\ \mathrm{kpc}, \tag{9}$$

$$\rho_c = 2 \times 10^{10} \left(\frac{M_h}{M_\odot}\right)^{-1/3} h^{-1/3} M_\odot\ \mathrm{kpc}^{-3}. \tag{10}$$

With these assumptions the gravitational potential of the halo is

$$\Phi_h(r) = 4\pi G\rho_c r_0^2 \left[\frac{1}{2}\log\left(1+x^2\right) + \frac{\arctan x}{x}\right], \tag{11}$$

where $x = r/r_0$. The galaxy has a circular velocity

$$v_c^2(r) = r\frac{\partial\Phi_h}{\partial r} = \frac{4\pi G\rho_c r_0^2}{x}(x - \arctan x); \tag{12}$$

The rotation curve increases rapidly in the inner parts of the galaxy, already being practically flat at $x = 1.5$.

In analogy with the DM component, we suppose that the gas extends out to a disk cut-off radius, ϖ_*. From a fit to the sample of dIs (discussed in Sec. 4) that we will use to test the model, it has been found that the HI radius-mass relation is well approximated by the law

$$\varpi_* = \varpi_0 M_{g,7}^{\alpha} \simeq 1.5 M_{g,7}^{0.338} \quad \text{kpc}, \tag{13}$$

where $M_{g,7} = M_g/10^7 M_\odot$. To obtain this relation we have in addition assumed that the ratio between the HI and the optical radius is ≈ 2. This is roughly consistent with the results of Salpeter & Hoffman (1996) who found a value 2.34 ± 0.14. We will use eq. 13 and the value $\varpi_0 = 1.5$ kpc throughout the paper, even if some uncertainty may still be present, as discussed in Sec. 6. For sake of clarity, it might be useful to give the explicit expressions for the relations among the three characteristic radii so far introduced in this Section. These are:

$$\frac{r_h}{\varpi_*} \simeq 1.23(\phi h^{-2})^{1/3} \tag{14}$$

$$\frac{\varpi_*}{r_0} \simeq 15.6 M_{g,7}^{-1/6}(\phi h)^{-1/2} \tag{15}$$

$$\frac{r_h}{r_0} \simeq 19.2 M_{g,7}^{-1/6}(\phi h^7)^{-1/6}. \tag{16}$$

In order to provide convenient expressions for the gas scale height H, number density $n_0 = \rho_0/\mu m_h$, and column density N_H, we assume that most of the mass is concentrated in a thin disk, producing a constant gravitational acceleration $g = 2\pi G\Sigma_t$, where $\Sigma_t = (M_g + M_h)/2\pi\varpi_*^2$ is the total matter surface density. Such a choice generates an exponential gas distribution with parameters given by the following formulae:

$$H = \frac{c_{s,eff}^2}{2\pi G\Sigma_t} = \frac{c_{s,eff}^2\varpi^2}{GM_g(1+\phi)} \simeq 2\left(\frac{\varpi_0^2}{\phi}\right) M_{g,7}^{2\alpha-1} c_{10}^2 \quad \text{kpc}, \tag{17}$$

$$n_0 = \frac{M_g}{2\pi H\varpi^2\mu m_h} \simeq 2\times 10^{-2}\left(\frac{\phi}{\varpi_0^4}\right) M_{g,7}^{2(1-2\alpha)} c_{10}^{-2} \quad \text{cm}^{-3}, \tag{18}$$

$$N_H = n_0 H \simeq 2\times 10^{20} M_{g,7}^{(1-2\alpha)}\varpi_0^{-2} \quad \text{cm}^{-2}, \tag{19}$$

where $c_{10} = c_{s,eff}/10$ km s^{-1}, $c^2_{s,eff} = c^2_s + \sigma^2$ is an effective sound speed, c_s is the gas sound speed; ϖ_0 is defined by equation (13) in kpc, and μ is the mean molecular weight. We have also assumed that $\phi \gtrsim 1$ to simplify the last expressions. We note that in this approximation, N_H is independent of both ϕ and $c_{s,eff}$ and, given that $1 - 2\alpha \simeq 1/3$, only weakly dependent on the visible mass of the galaxy.

2.1. Gas Mass

Eq. 1 describes the evolution of the galactic gas mass M_g. The gas content is decreased by star formation and outflow phenomena, at rates $\psi(t)$ and $W(t)$, respectively; it is increased by infall and stellar ejecta, at rates $A(t)$ and $E(t)$, respectively.

The star formation rate ψ has been suggested by different authors to depend on various quantities as the gas mass, column density or number density. We choose ψ, following Dekel & Silk (1987), to be proportional to the gas mass divided by the galactic free-fall time $t_{ff} = (4\pi G\rho)^{-1/2}$, where G is the gravitational constant: $\psi = M_g/\tau t_{ff}$; $\tau \simeq 160$ is the value appropriate to reproduce the actual star formation rate in the Milky Way. In addition to its simplicity, this formula represents the most natural scaling for the process and it can be physically motivated. We will see below as this expression results is a Schmidt-type law, modified by the presence of DM. The gas mass returned from stars, $E(t)$, depends on parameters as the stellar IMF, yield and return fraction, which are defined and discussed in Sec. 2.2.

The infall rate, $A(t)$, is very uncertain; for this reason most of our calculations assume no infall ($A(t) = 0$). We therefore presume that infall should not represent a major effect for low mass galaxies.

The term describing the gas outflow rate W is complex, and it is discussed in the following section, where we also introduce the distinction between blowout and blowaway processes.

2.1.1. Outflows

(a) Blowout

Both SNe and SBs may contribute to drive a substantial mass loss from the galaxy, but it is likely that SBs are more efficient due to their higher energy input; in the following we will mainly describe the SB case, but similar treatment applies to SNe. In order that mass previously located inside the region affected by the (multiple) explosion is ejected from the galaxy, the velocity v_b of the expanding shell has to be larger

than the escape velocity from the galaxy, v_e. The escape velocity can be calculated at the disk radius ϖ_* from the potential eq. 11:

$$v_e^2(\varpi_*) = 2|\Phi_h(\varpi_*)| \sim 8\pi G\rho_c r_0^2 \left[\frac{1}{2}\log(1+x_*^2) + \frac{\arctan x_*}{x_*}\right]; \quad x_* = \varpi_*/r_0. \tag{20}$$

Taking the appropriate value for x_*, as derived from eq. 14, the terms in parenthesis give a factor $\simeq 1.65$ for all galactic gas masses, since it is $x_* \gg 1$. It follows that

$$v_e(\varpi_*) \sim (13.2\pi G\rho_c)^{1/2} r_0 \sim 20 M_{g,7}^{1/3} (\phi h)^{1/3} \quad \text{km s}^{-1}, \tag{21}$$

Note that v_e is basically independent of ϖ_* as long as $x_* \gg 1$, which implies an almost flat $v_e(\varpi)$.

The evolution of a point explosion in an exponentially stratified medium, as the one introduced above, has been derived by Kompaneets (1960). This solution accurately approximates the exact numerical solution, (see for example MacLow *et al.* 1989) and can be obtained from dimensional analysis. It is useful to rederive it briefly in this context.

Suppose that the gas density distribution is horizontally homogeneous and $\rho(z) = \rho_0 \exp(-z/h)$. The velocity of the shock wave is $v \sim (p/\rho)^{1/2}$, where the pressure p is roughly equal to E/z^3; $E = NE_0$ is the total energy of the explosion, produced by N SNe in the association (we usually take $N \approx 100$), each of energy $E_0 = 10^{51}$ ergs. Then, it follows that

$$v(z) \simeq E^{1/2} \rho_0^{-1/2} e^{z/2h} z^{-3/2}. \tag{22}$$

This curve has a minimum at $z = 3H$ and this defines the height at which the shock wave, initially decelerating, is accelerated to infinity and a *blowout* takes place. Therefore we will use $3H$ as the fiducial height where the velocity $v_b = v(3H)$ is evaluated. Introducing the mechanical luminosity of the explosion, $L = E/t_{OB}$, where $t_{OB} \simeq 3 \times 10^7$ yr is the average lifetime of massive stars, we write eq. 22 as

$$v_b \simeq \left(\frac{e}{3}\right)^{3/2} L^{1/2} \rho_0^{-1/2} t_{3H}^{1/2} H^{-3/2}, \tag{23}$$

where t_{3H} is the time at which $z = 3H$. Unfortunately, the Kompaneets solution does not allow to estimate t_{3H} in a simple manner. For our purposes it is accurate enough to determine t_{3H} from solution for $v(t)$ given by Abbot *et al.* (1981) valid for a homogeneous atmosphere,

$$v(t) = \frac{3}{5}\left(\frac{125}{154\pi}\right)^{1/2} L^{1/5} \rho_0^{-1/5} t^{-2/5}, \tag{24}$$

from which follows

$$t_{3H} = (3H)^{5/3} \left(\frac{125}{154\pi}\right)^{-1/3} \left(\frac{L}{\rho_0}\right)^{-1/3}. \tag{25}$$

The final expression for v_b, obtained by substituting t_{3H} in eq.23, is then

$$v_b = \frac{e^{3/2}}{3^{2/3}} \left(\frac{125}{154\pi}\right)^{-1/6} \left(\frac{L}{\rho_0}\right)^{1/3} H^{-2/3} = 92 L_{38}^{1/3} (1+\phi)^{1/3} c_{10}^{-2/3} \quad \text{km s}^{-1}, \tag{26}$$

where $L_{38} = L/10^{38}$ ergs s^{-1} and we have used eqs. 17-18. Eq. 26 shows that the velocity at the re-acceleration point $z = 3H$ is inversely proportional to the scale height of the gas to the 2/3 power. As a consequence, thick gas layers will be able to prevent blowout. Note that H depends on σ (see eq. 17), in turn regulated by the SN energy input, as described by eq. 3.

There are three different possible fates for the SN-shocked gas, depending on the value of v_b. If $v_b^2 \leq c_{s,eff}^2$, where c_s is the sound speed in the ISM, the explosion will be confined in the disk and no mass loss will occur; for $c_{s,eff}^2 < v_b^2 < v_e^2$ the supershell will breakout of the disk into the halo, but the flow will remain bound to the galaxy; finally, $v_b > v_e$ will lead to a true mass loss from the galaxy. In the second case, it is likely that the hot gas will fall down again onto the disk, in a time scale comparable to the radiative cooling time

$$\tau_c \sim 3.2 \times 10^7 \left(\frac{T}{10^6 \text{K}}\right)^{1.6} \left(\frac{n}{10^{-3} \text{cm}^{-3}}\right)^{-1} \quad \text{yr}, \tag{27}$$

where T and n are the gas temperature and density, respectively. Since τ_c is much shorter than the typical chemical timescale ($\gtrsim 10^9$ yr), the delay on which the infall takes place with respect to the outflow is negligible, and to all purposes we can assume that the halo gas has always remained in the disk.

Once the blowout velocity v_b has been determined, the mass outflow rate can then be written as

$$W = \begin{cases} 0 & \text{if } v_b < v_e \\ 2\xi E_k^{(j)} \gamma^{(j)} v_b^{-2} & \text{if } v_b > v_e \end{cases} \tag{28}$$

Note the inverse dependence on v_b^2 of W: this simply reflects the fact that for a given driving energy $\propto \rho v_b^2$, slower outflows are more mass loaded. In the previous expression the kinetic energy injected by the source j (SNe or SBs) is $E_k^{(j)} = \eta E^{(j)}$, where η_j is an appropriate efficiency coefficient, that can be estimated from the assumed expansion law. For example, the expansion law given above has $\eta = 3/7$. However, for radiative bubbles, η is smaller and equal to about 3% (Koo & McKee 1992); we use this value throughout the paper.

Since part of the kinetic energy is used to accelerate material in the equatorial plane of the bubble, only a mass fraction ξ will leave the galaxy in the blowout. The actual value of ξ is relatively uncertain and model dependent. In a recent study MF have calculated, by means of a series of numerical simulations that assume a galactic structure identical to the one adopted here, the value of ξ in the range of mechanical

luminosities $L = 10^{37-39}$ ergs s^{-1} and galactic masses $M_{g,7} = 0.1, 100$. They find that in general the gas ejection efficiency in case of blowout is relatively small ($\xi \lesssim 7\%$). This conclusion has been obtained by keeping L_{38} fixed throughout the entire energy injection phase, and, more crucially, assuming a power-law dependence of ϕ on the mass of the galaxy given by PSS (eq. 4). Since here we try not to make any assumption on such relation, we choose to adopt the value $\xi = 0.07$, which should provide a reasonable estimate of the mass ejection fraction.

Finally, $\gamma^{(j)}$ is the explosion rate for the source i. For SBs it is $\gamma^{(SB)} = S(t) f_{_{OB}}/N_{SN}$, where $S(t)$ is the SN rate in the galaxy and $f_{_{OB}}$ is the fraction of SNe occurring in an association ($f_{_{OB}} \sim 0.7$). The analogous quantity for isolated SNe is $\gamma^{(SN)} = S(t)(1 - f_{_{OB}})$. The SN rate is obtained from $S = \nu\psi$, where ν is the number of SNe per unit mass of stars formed which can be calculated once a given IMF has been specified (see Sec. 2.2).

(b) Blowaway

By definition, the blowout phenomenon discussed above involves a limited fraction of the parent galaxy mass, the one contained in cavites created by the SN/SB explosion. A much more disruptive event may occur, *i.e.,* the blowaway, in which the gas content of the galaxy is completely expelled and lost to the intergalactic medium. In the following we derive in detail the necessary condition for the blowaway to occur.

We have seen (eq. 22-23) that blowout takes place when the at $z = 3H$ the shell velocity exceeds the escape velocity. Following the blowout the pressure inside the cavity drops suddenly due to the inward propagation of a rarefaction wave. The lateral walls of the shell, moving along the galaxy major axis will continue to expand unperturbed until they are overcome by the rarefaction wave at $\varpi = \varpi_c$, corresponding to a time t_c elapsed from the blowout. After that moment, the shell enters the momentum-conserving phase, since the driving pressure has been dissipated by the blowout. The correct determination of t_c requires the solution of a 5-th order algebraic equation (De Young & Heckman 1994). In an exponential atmosphere the shock wave moves faster in the vertical direction than in the equatorial one; hence the ratio of the vertical to equatorial velocity is $v_z(z)/v_\varpi = \exp(z/3H)$ and, when blowout takes place, $v_b = \exp(3/2)v_{\varpi_b}$. At the same moment, the radius of the shell in the plane is $\varpi_b = (2/3)H = bH$; the rarefaction wave is travelling at the sound speed of the hot cavity gas, $c_{s,hot}$. It follows from simple kinematic considerations that

$$\varpi_c \sim \varpi_b + \frac{v_{\varpi_b}}{c_{s,hot}}(3H + \varpi_c) = aH, \tag{29}$$

with a to be determined.

The requirement for the blowaway to take place is that the momentum of the shell (of mass M_c at ϖ_c)

is larger than the momentum necessary to accelerate the gas outside ϖ_c (of mass M_o)at a velocity larger than the escape velocity:

$$M_c v_{\varpi_c} \geq M_o v_e, \tag{30}$$

where $M_c = M_w + \pi(\varpi_c - \varpi_b)^2 \rho_0 H[1-(1/e)]$, $v_{\varpi_c} = v_b e^{-3/2}(\varpi_b/\varpi_c)^{3/2}$, $M_o = \pi(\varpi - \varpi_c)^2 \rho_0 H[1-(1/e)]$. Defining the axis ratio as $\epsilon = \varpi_*/H \geq 1$, substitution into eq. 30 yields the blowaway condition:

$$\frac{v_b}{v_e} \geq \frac{(\epsilon - a)^2 e^{3/2}}{[(1-\xi)a^2 + (a-b)^2]} \Big(\frac{a}{b}\Big)^{3/2}. \tag{31}$$

However, as $v_{\varpi_b}/c_{s,hot} \ll 1$ (see eq. 26), it follows that assuming $\varpi_c \simeq \varpi_b$, or $a \simeq 2/3$, is an excellent approximation for our purposes. Eq. 31 then becomes

$$\frac{v_b}{v_e} \gtrsim (\epsilon - a)^2 a^{-2} e^{3/2}, \tag{32}$$

if $\xi \ll 1$ as discussed above; eq. 32 is graphically displayed in Fig. 1. Flatter galaxies (large ϵ values) preferentially undergo blowout, whereas rounder ones are more likely to be blown-away; as v_b/v_e is increased the critical value of ϵ increases accordingly. Unless the galaxy is perfectly spherical, blowaway is always preceded by blowout; between the two events the aspect of the galaxy may look extremely perturbed, with one or more huge cavities left after blowout.

2.2. Chemical Evolution

Let us now consider the various terms appearing in eq. 2. As stated above the gas mass returned from stars, $E(t)$, is dependent on the IMF, φ, the return fraction, R (the fraction of the total mass transformed into stars which is subsequently ejected back into the ISM), and the net stellar yield, y (the total mass of an element ejected by all stars back into the ISM per unit mass of matter locked into stars). The IMF is of critical importance, since it determines the relative number of high mass (which eventually will end their life as Type II SNe) and low mass stars. However, its true nature is not well understood. Usually a single power-law function is used (there is little compelling evidence for a multi-component fit [Mateo 1988]; see also Padoan *et al.* 1997) with small differences among the most frequently used indexes. We follow this convention and assume a power-law form of the IMF, $m\varphi(m) \propto m^{-x}$, with x given below.

We next adopt the *Instantaneous Recycling Approximation*, (IRA) *i.e.,* stars less massive than 1 $M_\odot$ live forever and the others die instantaneously (Tinsley 1980), which allows E and E_i to be written respectively as

$$E = R\psi; \qquad\qquad E_i = [RX_i + y(1-R)]\psi; \tag{33}$$

note that Tinsley's eq. 3.14 contains a wrong extra factor $1 - X_i$, see Maeder (1992). The limitations of IRA are discussed by Tinsley (1980).

In order to quantify the above relation, we need to fix the value of R and y for the traced heavy element. We choose oxygen for the following reasons: *(i)* it is produced mainly in Type II SNe, which are also governing the mass loss and dynamics of the galactic ISM via their energy input; *(ii)* a large sample of dwarf galaxies with good quality abundance data for this species is available (see Sect. 4); *(iii)* oxygen yields have also been extensively studied by several authors (Arnett 1978, Woosley & Weaver 1986, Thielemann, Nomoto & Hashimoto 1992, Maeder 1992) and there is a good consensus about their dependence on the stellar mass. We therefore take $X_i \equiv X_o$, the oxygen mass fraction. The returned fraction and the net yield can be obtained using the standard formulae (Maeder 1992):

$$R = \frac{\int_{m_l}^{m_u} (m - w_m)\varphi(m)dm}{\int_{m_l}^{m_u} m\varphi(m)dm}; \qquad y = \frac{1}{(1-R)} \frac{\int_{m_l}^{m_u} m p_m \varphi(m)dm}{\int_{m_l}^{m_u} m\varphi(m)dm} \tag{34}$$

where the IMF φ is defined between the lower and upper masses $m_l = 1M_\odot$ and $m_u = 120M_\odot$, and w_m ($w_m = 0.7M_\odot$ for $m \leq 4M_\odot$ and $w_m = 1.4M_\odot$ for $m > 4M_\odot$) is the remnant mass (white dwarf or neutron star). The value of the power law index is $x = 1.35$ (standard Salpeter) and $x = 1.7$ (Scalo 1986). We have taken the oxygen stellar yield, p_m (*i.e.,* the mass fraction of a star of mass m converted into oxygen and ejected) from Arnett (1990). With these assumptions we obtain $R = (0.79, 0.684)$ and $y = (0.0871, 0.0305)$ for the (Salpeter, Scalo) IMF, respectively. We will present results only for the Salpeter IMF (although we have studied a few cases with the Scalo IMF) as differences are relatively minor and Salpeter's law seems to be currently better supported by a variety of observational evidences.

The previous values for the yields seem to be robust, although recent studies have pointed out that they might somewhat vary with metallicity. For example, using new stellar evolution models for $Z \approx 0.001$ ($1/20^{\rm th}$ solar) and $Z \approx 0.02$ (solar), which include new opacities, Maeder (1992) calculated stellar yields for, among other species, oxygen as a function of metallicity and the expected mass limit for the creation of black holes. The stellar models take into account metal dependent opacity and nuclear effects, changes of mass loss rate with metallicity and moderate core-overshooting. Yields of heavy elements tend to decrease with stellar mass if a black hole is formed, because in this case heavy elements are partially swallowed by the black hole. This effect is less important at high metallicities, because most metals escape in a stellar outflow before the collapse to a black hole. In order to include these findings, at least in an approximate manner, we have used interpolated Maeder's results for case C (minimum mass for formation of the black hole equal to 22 $M_\odot$) yields. For a Salpeter IMF the value of the yield agrees with the one obtained

from Arnett's results at metallicity $\approx 15\%$ of solar, but it is smaller for lower metallicities. We have done numerical runs of our models using both prescriptions and we found differences of the order of 30% in the final metallicity.

A particularly important quantity depending on the IMF is the number of SNe per unit mass of stars formed, ν. For a Salpeter IMF with $m_l = 1M_\odot$ and $m_u = 120M_\odot$, we obtain $\nu^{-1} = 53M_\odot$. It is worth pointing out, though, that ν is rather sensitive to the adopted value of m_l.

Finally, we are making the hypothesis that the oxygen abundance in the outflow is the same as in the ISM, *i.e.,* we are not considering metal-enhanced outflows. The reason for this assumption is the following. MF have determined, in addition to the gas ejection efficiency as discussed in the previous Section, the metal ejection efficiency per SB in a dwarf galaxy, ξ_Z. Let us consider a typical case among the ones simulated in their paper, *i.e.,* $L_{38} = 1$, $M_{g,7} = 1$, for which they obtain $\xi = 1.4 \times 10^{-2}$ and $\xi_Z = 1.0$. If the amount of heavy elements produced per SN is $\approx 3M_\odot$, then during the energy injection phase lasting 50 Myr, about $470M_\odot$ of metals are diluted with the ejected gas, if mixing between the two components is fast enough. This corresponds to an increase in the metal abundance of the outflow of $\approx 3 \times 10^{-3}$, which is at least comparable if not smaller, than the typical abundances of dIs, as can be appreciated by inspecting our control sample in Tab. 1. This should demonstrate that metal enhanced outflows can be produced only in the very early stages of the evolution. In addition the above argument does not take into account the interaction with the hot cavity gas which strengthens this conclusion. Of course, if all the metals produce in a SB escape from the galaxy as in the case just considered, there would be no way for the galaxy to become metal enriched. However, the results of MF allow to conclude that the metal enrichment is mostly due to low-luminosity SBs and/or isolated SNe, which do not blowout and for which ξ_Z is strongly reduced.

2.3. Kinetic Energy Balance

Finally, we consider the kinetic energy balance, eq. 3. As we have seen in previous Sections, SNe and SBs are responsible for the mass outflow from the galaxy. On the other hand, they also contribute to the turbulent pressure of the ISM. Turbulent motions sustained by SN mechanical energy input (for a derivation of the turbulent spectrum in the ISM, see Norman & Ferrara 1996) can be dissipated via radiative losses during cloud-cloud collisions. Eq. 3 expresses the rate of change of the kinetic energy density in the ISM, $\epsilon_k = \rho\sigma^2$, as determined by the turbulent energy sources and sinks. The rate at which ϵ_k increases following

SNe and SBs explosions is

$$\dot{\epsilon}^{+} = \frac{\rho}{M_g}\left[E_k^{(j)}\gamma^{(j)}(1-\xi)\right] = 1.2\times10^{-28}\left(\frac{\phi}{\varpi_0^4}\right)^{3/2} M_{g,7}^{3(1-2\alpha)}(c_s^2+\sigma^2)_{10}^{-3/2}. \quad (35)$$

Note that eq. 35 is strictly valid only for $\phi \gtrsim 1$, due to the approximations made in eq. 17-18. The dissipation rate per unit volume $\dot{\epsilon}^{-}$ is the product of three quantities: the energy lost per collision, ΔE, the number density of clouds in the galaxy, N_c, and the cloud-cloud collision frequency, ω_c. If $R_c \approx 5$ pc is the cloud radius, then $N_c = 1/\pi R_c \lambda_{mfp}$, where $\lambda_{mfp} \approx 0.13$ kpc is the mean free path for cloud-cloud collisions; these values are conservatively assumed to be the same as in the Milky Way (Spitzer 1978). Then, the collision frequency is $\omega_c = \sigma/\lambda_{mfp}$. In general, one should integrate the dissipation rate over a cloud velocity distribution; for simplicity, we assume that all clouds move with the same velocity dispersion σ. The maximum energy loss per collision ΔE takes place when the collision is inelastic: for two clouds of mass m_1 and m_2 moving with relative velocity $\Delta\mathbf{v} = \mathbf{v_1} - \mathbf{v_2}$ this corresponds to

$$\Delta E = \frac{1}{2}|\Delta v|^2 \frac{m_1 m_2}{m_1+m_2}. \quad (36)$$

Given the present uncertainty on the determination of the mass spectrum of diffuse clouds in dwarf galaxies, we assume that all clouds have the same mass, m. It follows that $\Delta E = m\sigma^2$, *i.e.,* all the initial kinetic energy is lost. Are cloud collisions in dwarfs truly inelastic ? The elasticity of collisions (defined as the ratio of the final to the initial kinetic energy of the clouds) has been recently studied by Ricotti *et al.* (1997). Among other results, the authors find that the elasticity depends both on metallicity and on cloud size; nevertheless, most conditions are found to lead to inelastic collisions, in the absence of a magnetic field. In two subsequent papers, Miniati *et al.* (1997, 1999) pointed out that even a relatively weak magnetic field makes collisions much more elastic. In fact, if a magnetic field is present, a considerable fraction of kinetic energy can be stored in the bending modes of the field and returned to the clouds after the collision. The result is in a quasi-elastic collision with a much smaller net dissipation. Including all the detailed physics they considered would greatly complicate the present picture, let alone our ignorance about magnetic fields in dwarf galaxies. To roughly take into account this effect, we have adopted a reduction factor $b_1 \lesssim 1$ in the energy dissipation rate. Hence it is

$$\dot{\epsilon}^{-} = b_1 N_c \omega_c \Delta E = 2.1\times10^{-28} b_1 \left(\frac{\phi}{\varpi_0^4}\right) M_{g,7}^{2(1-2\alpha)} \sigma_{10}^3 (c_s^2+\sigma^2)_{10}^{-1}. \quad (37)$$

Fig. 2 shows the velocity dispersion equilibrium value, σ_{eq} obtained by equating $\dot{\epsilon}^{+}$ to $\dot{\epsilon}^{-}$ (for $b_1 = 1$) as a function of galactic gas mass and for different values of ϕ. These curves represent the limiting case in which $c_{s,eff}$ is dominated by turbulence, *i.e.,* c_s is negligible with respect to σ. Then the above inequality holds

to a good approximation for dwarfs galaxies and the equilibrium value for σ is given by

$$\sigma_{eq} \simeq 4.5 b_1^{-1/4} \left(\frac{\phi}{\varpi_0^4}\right)^{1/8} M_{g,7}^{(1-2\alpha)/4} \mathrm{km\ s^{-1}}. \tag{38}$$

The equilibrium value of the cloud velocity dispersion increases with galactic gas mass as a result of the more vigorous star formation activity occurring in those objects. Also, the spread introduced by the different DM content is about a factor 2 only for a given galactic mass. This allows us to conclude that the *gas velocity dispersion is only mildly influenced by the underlying gravitational potential of the galaxy.* Instead, the relatively similar values commonly observed in galaxies greatly differing in mass, suggest that self-regulation is at work through the processes described in this Section.

It is instructive to calculate the time necessary to reach equilibrium, $t_{eq} = \sigma_{eq}^2 |d\sigma^2/dt|^{-1}$, for the velocity dispersion:

$$t_{eq} = 10^7 \left(\frac{\phi}{\varpi_0^4}\right)^{-1/2} M_{g,7}^{(2\alpha-1)} \sigma_{10}^2 (c_s^2 + \sigma^2)_{10} \text{ yr}. \tag{39}$$

This short timescale implies that the memory of the initial gas dynamical conditions is washed away very rapidly and, since (see eq. 44 below), the chemical evolution timescale is much longer than t_{eq}, using σ_{eq} is an excellent approximation for several purposes.

3. Analytical Insights

Before we present the numerical results in the next Section, we discuss a few limiting cases that can provide some physical insight into the problem. We have seen that t_{eq} is much smaller than the chemical evolutionary timescale; this motivates the approximation $d\epsilon_k/dt \simeq 0$. Assuming in addition $A(t) = 0$, the system eqs. 1-3 is reduced to

$$\frac{d}{dt} M_g(t) = -\psi(t) + E(t) - W(t), \tag{40}$$

$$\frac{d}{dt}[X_i(t) M_g(t)] = -X_i(t)\psi(t) + E_i(t) - X_i W(t), \tag{41}$$

or, substituting the expressions given in the previous Section for the various terms,

$$\frac{d}{dt} M_g(t) = (R-1)\psi(t) - W(t), \tag{42}$$

$$M_g \frac{d}{dt}[X_i(t)] = -y(R-1)(1-X_i)\psi. \tag{43}$$

From eq. 43 one can see that the oxygen fraction evolution does depend on the outflow rate only through the changes in M_g, in turn regulated by the outflow. Integration of eq. 43 yields

$$X_i(t) = 1 - [1 - X_i(0)] e^{y(1-R)/\tau t_{ff} t}. \tag{44}$$

The chemical evolution timescale is $t_e \simeq t_{ff}\tau/y(1-R)$, which for the parameters adopted here is $\approx 9\times 10^3 t_{ff} \gg t_{eq}$, which justifies our statement after eq. 39. By eliminating time between eqs. 42-43, we can write

$$M_g \frac{dX_i}{dM_g}[(R-1)\psi - W] = -y(R-1)(1-X_i)\psi, \tag{45}$$

Note that, unlikely for dX_i/dt, $X_i(M_g)$ is a function of the outflow rate W. Since $R-1$ is always negative, the l.h.s. cannot vanish for any value of W.

3.1. No Outflow case: $W = 0$

When $W = 0$, eq. 45 has the simple solution

$$X_i(M_g) = 1 - [1 - X_i(0)] \left[\frac{M_g}{M_g(0)}\right]^y. \tag{46}$$

3.2. Constant Outflow case: $W = \text{const.} \neq 0$

The solution of eq. 45 for the case $W \neq 0$, (but constant) is

$$X_i(M_g) = 1 - [1 - X_i(0)] \left[\frac{KM_g - 1}{KM_g(0) - 1}\right]^y, \tag{47}$$

where $K = (1-R)/t_* W$ and $t_* = \tau t_{ff}$. Since $t_* W$ is the amount of gas ejected during a star formation timescale, KM_g expresses the ratio between the mass of gas that goes into stars and the gas loss via the outflow. Hence large values of $|K|$ refer to negligible ejection rates, whereas for small K outflow mass loss dominates. Of course, eq. 47 reduces to eq. 46 in the limit $|K| \to \infty$.

3.3. Are Outflows Important ?

The metallicity of a dwarf galaxy is closely related to the amount of gas consumption; it is then important to assess the relative importance of the two main processes involved in the latter, namely star formation and outflows. A straightforward answer can be obtained by comparing the two r.h.s. terms in eq. 42. Outflow mass losses will be dominant if

$$(1-R)\psi \ll W = 2\xi E_k^{(j)} \gamma^{(j)} v_b^{-2}, \tag{48}$$

or

$$v_* = \left[\frac{2\xi\eta\nu E_0 f_{_{OB}}}{(1-R)}\right]^{1/2} \gg v_b, \tag{49}$$

where v_* is a characteristic velocity associated with the energy injection by star formation, via SN explosions, into the ISM: for the parameters adopted in this paper, $v_* \sim 115$ km s^{-1}. We now made the following simplifying hypotheses: *(i)* the mass loss induced by isolated SNe is negligible; *(ii)* velocity dispersions are supersonic: $c^2_{s,eff} = c_s^2 + \sigma^2 \simeq \sigma^2$ (see Fig. 2); *(iii)* the velocity dispersion has its equilibrium value. With these assumptions, we can derive an explicit expression for v_b by substituting eq. 38 into eq. 26:

$$v_b = 101\ L_{38}^{1/3} b_1^{1/6} \phi^{1/4} \varpi_0^{1/3} M_{g,7}^{(2\alpha-1)/6} \quad \text{km s}^{-1}, \tag{50}$$

We can now determine the regions in the $(1+\phi) - M_{g,7}$ plane where outflows dominate over mass consumption ($v_* > v_b$), along with the blowout ($v_b > v_e$), and blowaway (eq. 32) conditions. In terms of the previous expressions, these three conditions translate into:

$$\textit{Blowout} \rightarrow \phi \lesssim 5 \times 10^{10} L_{38}^4 b_1^2 \varpi_0^4 M_{g,7}^{2(2\alpha-3)} h^{-4/3}; \tag{51}$$

$$\textit{Blowaway} \rightarrow \phi \lesssim 0.27 \left[L_{38}^{1/3} b_1^{-5/6} \varpi_0^{1/3} M_{g,7}^{(\alpha/3-3/2)} h^{-1/3}\right]^{12/19}. \tag{52}$$

$$\textit{Outflow dominates} \rightarrow \phi \lesssim 0.3 L_{38}^{-4/3} b_1^{-2/3} \varpi_0^{-4/3} M_{g,7}^{2(1-2\alpha)/3}; \tag{53}$$

These relations provide a qualitative understanding of the various fates of a dwarf galaxy (*i.e.,* closed box evolution, blowout, blowaway, gas consumption) and are graphically displayed in Fig. 3. in which we have fixed $L_{38} = 1, b_1 = 1$. *Galaxies with gas mass content larger than* $\approx 10^9 M_\odot$ *do not suffer mass losses, due to their large potential wells (a result also found in the numerical simulations by MF).* Of course, this does not rule out the possible presence of outflows with velocities below the escape velocity (fountains) in which material is temporarily stored in the halo and then returns to the main body of the galaxy, as discussed in § 2. For galaxies with gas mass lower than this value, outflows cannot be prevented. If the gas mass is reduced further, and for $\phi \lesssim 20$, a blowaway, and therefore a complete stripping of the galactic gas, should occur. Just as an example, we have plotted the expected value of ϕ as a function of M_g, as empirically obtained by PSS (eq. 4), which should at least give an idea of a likely location of the various galaxies in the plane of Fig. 3. If dwarfs are a one parameter family with respect to these quantities, they should align along the dotted line, and the transition from blowout to no mass loss regime should occur at $M_{g,7} \approx 100$.

Eq. 53 indicates that the predominant mechanism of gas consumption is provided by the conversion of gas into stars, even when an outflow takes place. In fact, given the dependence of eq. 53 on the gas mass, in larger galaxies (*i.e.,* $M_g \gtrsim 10^9 M_\odot$) outflow losses could in principle dominate, but the previous discussion shows that in such systems blowout - and consequent mass loss - cannot occur. The reason for this behavior is that driving a wind is a relatively inefficient process: the mass of gas that has to be transformed in stars is always larger than the mass of gas ejected by the energy available to drive the outflow produced by the same stars. We conclude that *the main source for gas consumption is provided by star formation*, in agreement with Davies & Phillips (1988).

The previous results do not analyze the changes in the gas content of the galaxy during its evolution; Fig. 3 is meant to give a simple schematic overview of the most important physical processes and of their approximate domains. The detailed discussion of the fully, time-dependent results is given in Sec. 4.

3.4. A Dark Matter-Modified Schmidt law

Using relations 17-18 we can rewrite eq. 42 explicitly as

$$\frac{d}{dt}M_g = A M_g^{3/2} M_T^{1/2} c_{s,eff}^{-1} - W(t) \tag{54}$$

where $A = \sqrt{2}(R-1)G/\tau\varpi_*^2$. The additional assumption of a steady state for σ allows to eliminate the velocity dispersion (contained in $c_{s,eff}$) from eq. 54. The first term represents the mass consumption due to star formation, and the second describes the mass loss in the outflow, if present. It is interesting to note that the expression for star formation rate resembles a standard Schmidt power law, but with the relevant difference that it depends both on the gaseous *and* the total mass. This may have important observational consequences, as it will become clear from the results presented in § 4. In the absence of DM ($M_T = M_g$) the star formation law power index, assuming equilibrium for σ, would be equal to $(7+2\alpha)/4 = 1.92$.

4. Available Observations

We are able to perform different tests of our models against data available in the literature. We can compare model predictions against a relatively large sample of nearby gas-rich dwarf galaxies. Since our predictions relate to on-going star formation in galaxies with an ISM, we necessarily select galaxies which are gas rich. The aim is to test as much of the parameter space as possible to verify the general predictions of the models. We consider in addition a uniform sample of low surface brightness, gas-rich galaxies, which

are underluminous systems for their HI content (van Zee *et al.* 1997a,b). We finally model in detail the very carefully studied nearby galaxy Leo A, for which in particular the star formation history is well constrained.

Combining observations from many different sources has the difficulty of numerous different definitions. We have tried to make sure that the data which we use come from equivalent measures. We define the total mass of a galaxy as the sum of the gas mass, the stellar mass, and the DM mass. We thus define the DM mass to be the short-fall between the total mass and the visible mass (stars plus gas) mass. Measuring the integrated photometric and structural properties of nearby galaxies is not a trivial task. The size range goes from arcmins to many degrees, and nearly all of the galaxies in our sample have low surface brightness which complicates reliable and consistent surface brightness measures. A number of the smallest dwarf irregular galaxies are dominated by random motions rather than rotation, which makes disentangling the different velocity components, and determining the total mass especially difficult. Sometimes it is unclear if the HI observed is in virial equilibrium.

4.1. The "Skillman" Nearby Galaxy Sample

Table 1 compiles the results from a number of relatively well studied nearby galaxies. The selection of these galaxies is such that they contain HII regions bright enough to obtain spectroscopy for oxygen abundance determinations, *i.e.,* with published 12+ log [O/H]. These mostly come from Skillman, Kennicutt & Hodge (1989), hence the name of the sample, and then a few more recent results were also included. The majority of the metallicities in the Skillman *et al.* paper did not include errors, so the values given in Mateo (1998) were used. Then the literature was searched for the other parameters of interest, namely HI mass, total dynamical mass, and surface brightness. It was difficult to find reliable measures of the ISM velocity dispersion in these galaxies, and some of the values are of dubious accuracy, and with a few exceptions, which are indicated, most of the σ_{ISM} should be treated as upper limits as well. There were also a number of different definitions of surface brightness determinations, which are intrinsically difficult measurements for low surface brightness irregular galaxies. These, in certain indicated cases, should be considered as upper limits. Often, when looked at in detail, a galaxy is found to contain an extremely extended low surface brightness halo (e.g. Minniti & Zijlstra 1996). The (total) dynamical mass of many of the galaxies in this sample comes from single-dish observations by Huchtmeier & Richter (1988), using the HI linewidth versus optical diameter relation defined by Casertano & Shostak (1980). The footnotes of Table 1 should be carefully noted, as they provide an estimate of the true reliability of each measure.

4.2. The "Van Zee" Low Surface Brightness Dwarf Sample

Another comparison with our model comes from the detailed self-consistent work of van Zee *et al.* (1997a, b) on a sample of galaxies defined by unusually large M_H/L_B values. The sample includes isolated HI rich galaxies with extended HI envelopes located around low optical luminosity spiral galaxies, and comparison "normal" dwarf galaxies. The normal dwarfs have similar star formation rates and other global properties to the low surface brightness sample, but they are less massive. The gas dynamics and kinematics of most of these galaxies were then studied in great detail, as were the young stellar population (via colors and metallicities of HII regions), and metallicities were also measured by van Zee. Thus, this is a good comparison sample for our models even though the galaxies have slightly higher mass and larger physical scale than the single cell type galaxies which make up the majority of the Skillman sample. The values are given in Table 2. There is one galaxy which overlaps with the Skillman sample (DDO 187).

4.3. An Individual Case: Leo A

Focusing even further in on our model predictions we now make a detailed comparison with the known star formation history (SFH) and metallicity of a nearby dI galaxy, Leo A, which is part of the Skillman sample, and has a even lower surface brightness than typical for the Van Zee sample. We choose Leo A because it has one of the most detailed SFH available for a low surface brightness, dwarf irregular type galaxy (Tolstoy *et al.* 1998). The SFH is reasonably well determined from stellar color-magnitude diagrams (CMD) studies. Such studies (Tolstoy & Saha 1996, Tolstoy *et al.* 1998, Tolstoy 1998b) are able to accurately trace the SFH using several indicators derived from theoretical stellar evolutionary tracks.

5. Comparisons with Samples

We first consider how the model predictions fit in with the global properties of nearby gas-rich galaxies.

5.1. Oxygen Abundance

Fig. 4 shows a comparison between the data and the model results for the oxygen abundance as a function of the final gas mass M_g^f for different values of ϕ. As a general trend, the oxygen abundance in the samples of dwarf galaxies, listed in Tables 1 and 2, increases with M_g^f: this behavior is correctly reproduced

by our results. However, for a given M_g^f, there is a considerable spread in the metallicity data. Assuming that galaxy interactions have not played a significant role in the evolution of any of these systems, then this can be understood as an effect of the different DM content, where *higher dark-to-visible mass ratios produce higher final values of* X_o. This is due to the fact that as the DM content is increased at fixed gas mass, the gas tends to be compressed towards the central regions by the stronger gravitational potential. As a consequence of the higher density, the star formation process is favored and its rate increased. For similar reasons, adding DM makes outflows, and hence oxygen mass loss, less efficient.

From Fig. 4 it appears that almost all sample galaxies *can be inferred to have dark-to-visible mass ratio* $\phi \simeq 0 - 30$ (although about 65% of the objects have $\phi \leq 10$ as shown by the observed distribution in Fig. 5), in order to explain the observed oxygen abundances. The values of ϕ derived from the model are also reported and the two distributions are seen to be in good agreement.

The sample of galaxies have gas masses in the range $10^7 - 10^{10} M_\odot$. The lower limit is consistent with our model limit at which less massive objects cannot survive blowaway, as indicated by the absence of low ϕ galaxies below $10^7 M_\odot$. For these extremely small objects a considerable amount of DM is required to prevent blowaway, as already noted in Sec. 3. Thus, a prediction of the model is *the existence of a lower limit for the oxygen abundance* of small mass ($M_g^f \lesssim 10^7 M_\odot$) dI: almost independently of ϕ, $X_o^{min} \approx 0.02$ (*i.e.,* $12 + \log(O/H) \approx 7.2$). This lower limit is set by the minimum amount of DM necessary to avoid the blowaway, which results in the minimum metallicity. We expect that dI galaxies with $X_o < X_o^{min}$ should not be observed since they are likely to be disrupted during the initial phase of star formation. It is possible that today's dSph/dE galaxies could be the remnants of such a catastrophic event, consistent with dE galaxies typically being dominated by old stars and being extremely metal poor; we will discuss these issues in more detail in Section 6.

It is interesting to note that, there is a group of objects with masses around $10^7 M_\odot$ that should be critically close to fulfill the blowaway condition. The fact that these objects are among the faintest star forming objects known is consistent with the destruction of even smaller galaxies in the past.

5.2. Mass Outflow Rate

Most dwarf galaxies are predicted to evolve through an outflow phase in which a fraction of the gas is injected in the intergalactic medium (Wyse & Silk 1985, Vader 1986, 1987). In general, we find that the

outflow mass loss in a galaxy is a decreasing function of time and that single SN events are not powerful enough to drive a significant outflow. Fig. 5 shows the behavior of the mass outflow rate $\langle \dot{M}_w \rangle$, averaged over the entire evolutionary time. The *mass loss rates are in the range* $10^{-5} - 0.04\ M_\odot\ yr^{-1}$. The mass loss is a rather steep function of gas mass peaking at $M_g^f \approx$ few $\times\, 10^8 M_\odot$. The peak is the product of two effects: on the one hand the galaxy has to be sufficiently gas rich to form enough massive stars to power the outflow; on the other hand, larger masses correspond to higher escape velocities which make the outflow increasingly difficult. For a given galaxy gas mass, $\langle \dot{M}_w \rangle$ is only weakly dependent on the dark-to-visible mass ratio, as can be appreciated from Fig. 6, which shows the comparison between the three cases $\phi = 0, 30, 300$. Consistently with the above interpretation, $\langle \dot{M}_w \rangle$ decreases with increasing ϕ; however, the differences between the cases $\phi = 0$ and $\phi = 300$ are less than a factor $\lesssim 10$ in the mass range considered; at the high mass end the larger v_e quenches the blowout (see Fig. 3). Galaxies of mass few $\times\, 10^8 M_\odot$ are therefore the *major pollutants of the IGM with both mass and heavy elements.*

5.3. Gas Velocity Dispersion

As SNe are the most important oxygen source, and they also regulate the kinetic energy input to the ISM, it is natural to investigate the relationship between σ and X_o in galaxies. Such a relationship, as obtained from our model, is shown and compared with available data in Fig. 7 for three different values of $\phi = 0, 10, 100$ which result in different M_g^f (compare with Fig. 4). This relationship is surprisingly tight, in the sense that dI galaxies with higher metallicity tend to show higher velocity dispersions, at least for the uniformly measured van Zee sample. As said above, there are general reasons to expect such trend, but the interesting aspect is that all galaxies *independently of their DM content fall on the same* $X_o - \sigma$ *curve, which has the rather steep slope 3.5*, as seen from the fitting curve drawn on top of the points in Fig. 7. Several independent processes concur to establish this relation and their detailed interaction is not easy to disentangle. Ultimately, however, the most important factor is the interplay of DM and SN feedback in regulating both the chemical and kinetic energy balance of the ISM. However, the magnetic field is also an important ingredient as it can result in more elastic, and hence less dissipative, cloud collisions. Inclusion of a magnetic field does not modify the above relation between metallicity and gas dispersion, but it could shift it to larger values. This effect is quantified in Fig. 7 where we have drawn the analogous curves for three different values of b_1, the magnetic reduction factor introduced in eq. 37 (this is the only case in which we explore b_1 values different from 1). *A reduction in the cloud collision energy dissipation rate seems to*

fit better the data, with a preferred value $b_1 \approx 0.5$. This means that about half of the kinetic energy of the clouds is temporarily stored into magnetic line tension and it is released again after the collision, consistent with the findings of Miniati *et al.* (1999).

5.4. Surface Brightness

Our models must also be able to reproduce, at least to first order, the observed properties of the sample stellar populations. Here we start from the surface brightness - visible (*i.e.,* disk gas + stars) mass relation. At the present stage, we are able to compare our results with the data only at a basic level since a detailed comparison would require a self-consistent computation of the photometric evolution of the galaxy. However, as a sanity check, it is important to get at least an approximate estimate of the surface brightness.

To this aim we use the results obtained by PSS, who have investigated the structural properties of a sample of 1100 spiral galaxies using optical and radio rotation curves and relative surface photometry. According to these authors, the relationship between the visible mass and the B-band luminosity of a galaxy has the following expression (solar units):

$$\log\left(\frac{M_v}{L}\right) = 0.5 + \left[0.35\log\left(\frac{L}{L_\star}\right) - 0.75\log^2\left(\frac{L}{L_\star}\right)\right]. \tag{55}$$

By applying this formula, and assuming the usual mass-radius relationship as given by eq. 13 and a disk mass-to-light ratio of 0.5, we have derived the surface brightness of the model galaxies. The comparison between the theoretical and observational data points, shown in Fig. 8 for different values of ϕ, indicates a satisfactory agreement within the limitations mentioned above. The general trend of increasing surface brightness with gas mass is successfully reproduced as well as the typical range of values. Given the assumptions made, we do not emphasize this result any further. As a final remark, one has to keep in mind that the extrapolation of the empirical relation eq. 55 to the mass range relevant to the least massive dwarfs is at this stage only very tentative. The upper points in the figure are all "bursts", or BCD type galaxies, which are likely to possess faint underlying halos which have not been included in the surface brightness measures, making it an upper limit. As we argue several times in this paper, these burst episodes affect only mildly the global evolutionary properties of dwarfs, although the increased luminosity during these periods might allow their detection at cosmological distances (see Section 6).

5.5. Star Formation History

The presence of DM profoundly influences the star formation history of dwarf galaxies. Its main influence is on the processes regulating the star formation rate is via the compression of the cool gas in a deeper gravitational potential, thus increasing the mean gas density. We have computed the star formation rate for galaxies with different gas masses ($M_g^f \approx 10^8 - 10^9 M_\odot$) and values of $\phi = 0, 30$. Our model assumes that galaxies are evolving in a relatively undisturbed manner, as we are not considering any external (or internal) perturbation which could trigger vigorous star forming episodes. The behavior of the star formation rate in time for the set of model galaxies above is shown in Fig. 9. The rates tend to decrease in time as the gas is either consumed by star formation (predominantly) or lost in the outflow. The variation of the gas mass is relatively modest though, being within a factor 2-3 of the initial value, independently of the amount of DM. As more DM is added, it increases the star formation rate. *For a* $M_g^f \approx 10^9 M_\odot$ *the star formation rate is in the range* $2 \times 10^{-3} - 0.07\ M_\odot yr^{-1}$*, depending on the evolutionary stage and on its dark-to-visible mass ratio.*

5.6. A Specific Case: Leo A

The SFH obtained by Tolstoy *et al.* (1998) for Leo A is shown in the upper panel of Fig. 10 (solid curve). Essentially one major star formation episode ($\approx 5 \times 10^{-4} M_\odot$ yr^{-1}) appears to have occurred about 1.5 Gyr ago lasting 0.6 Gyr, preceded by a long lasting low level of star formation similar to that observed today. This older star formation activity is poorly constrained by current data. For the long-lasting (≈ 11 Gyr) interval before the burst, only an upper limit of about $\approx 1.7 \times 10^{-4} M_\odot$ yr^{-1} can be set. This is broadly consistent with variations about a constant (but low) level.

We make two comparisons with our models. We input the Tolstoy *et al.* SFH for Leo A into our model, and predict the resulting metallicity. We also compare the SFH and the final metallicity predicted by our model with the gas mass and dark-to-visible mass ratio taken from the observations of Leo A, independently of what is known about the SFH.

For the first case we obtain the metallicity evolution for Leo A (see bottom panel of Fig. 10). In order for the final metallicity ($12 + log[O/H] = 7.2 \pm 0.1$) to agree with the observed value ($12 + log[O/H] = 7.3 \pm 0.1$, it is necessary to assume that in the latency period star formation has proceeded at a rate equal to the upper limit set by observations ($\approx 5 \times 10^{-4} M_\odot$ yr^{-1}); a lower level of star formation would underproduce

the observed oxygen abundance. Alternatively, one could possibly explain the metallicity of the galaxy by postulating an extremely early burst, *i.e.,* in the first 2 Gyr, which cannot be detected by present observations. Given these uncertainties, we show only the fit to the data that is based on available data. The combined metallicity evolution – CMD information clearly provides useful constraints on the SFH in galaxies; thus, it will be interesting in the future to check if more sensitive observations will allow to decide between the two above possibilities.

Next, we have run our code with the standard prescriptions, *i.e.,* without assuming the SFH is known *a priori*, for the specific case of Leo A. We obtain a metallicity $12 + log[O/H] = 7.38$. Of course, the derived SFH differs from the inferred one (an obvious consequence of the fact that we have not attempted to allow for significant variations in star formation rate), but it apparently approximates the mean of the one inferred from observations and we regard this as a success of the model.

6. Remarks and a Possible Scenario

The model presented in this paper provides a consistent, interpretation of the behavior and properties of dwarf galaxies. However, it is important to discuss the uncertainties associated with our analysis. There are at least three quantities that we consider poorly constrained and which might influence our results: *(i)* the HI radius - mass relation, *(ii)* the strength of the magnetic field and *(iii)* the oxygen chemical yield.

Various authors have found/used different dependences of the HI radius of dwarfs as a function of their HI mass. For example, Matteucci & Chiosi (1983) from a linear fit of a sample containing 45 BCD/dI galaxies derived the dependence $\varpi_* = 0.96 M_{g,7}^{2/3}$ kpc (using the same factor of 2 as here for the HI-optical radius conversion). Although the coefficient ϖ_0 is roughly similar, the curve is sensibly steeper. A detailed study by Salpeter & Hoffman (1996) of 70 BCDs/dIs yielded a slope $\alpha \approx 0.5$ for the relation between the geometric mean of the outermost HI radius and the optical radius and the HI mass. The van Zee sample, which is biased towards low surface brightness objects, has an even flatter slope, $\varpi_* \propto M_{g,7}^{0.3}$. Clearly these measures are difficult as they depend on the ability to trace extended HI distributions. In spite of these uncertainties, it is reassuring to find an excellent agreement between our adopted relationship eq. 13 and the one derived from the independent sample of 49 spiral galaxies with extended HI disks by Broeils & van Woerden (1994). The comparison between the data and the analytical relation eq. 13 (not a fit!) is shown in Fig. 11 and, although the latter has been derived from a sample of dwarf galaxies, it clearly holds for larger objects. Our models are only mildly affected by this uncertainty. As a rule of thumb, larger

values of α with respect to the one adopted here (0.338, see eq. 13) would produce a flatter metallicity – mass/luminosity relation; a larger ϖ_0 would instead shift such a relation towards smaller metallicities. Correlation statistics based on larger samples are needed to completely clarify this issue.

We have also predicted the existence of a tight relation between gas velocity and metallicity in dwarfs (it is interesting to note that an analogous relationship has been recently found between the stellar velocity dispersion and metallicity in four dSphs by Richer *et al.* 1999). The agreement with the data is very good, particularly if a kinetic energy dissipation during cloud collisions by about a factor of 2 is allowed. This can be easily achieved, under a variety of collision conditions (ranging from adiabatic to radiative cases) if a magnetic field is present. The elasticity of the collision (defined as the ratio of the final to the initial kinetic energy of each cloud) is enhanced by the above required factor 2 for a magnetic pressure equal to about 1/4 of the gas pressure in the ISM (Miniati *et al.* 1999); we recall that this ratio in the Galaxy is around unity. Our knowledge of the magnetic field strength and configuration in dwarfs is still relatively scarce. The most complete survey aimed at the determination of the B strength in dwarf LSBs has been presented by Klein *et al.* (1992). These authors, using Effelsberg 100-m observations at 4.75 GHz, report typical B strengths $\lesssim 2 - 4\mu$G for seven dIs in their sample. Although this conclusion is subject to several caveats due to the assumptions made to derive it, Klein *et al.* conclude that these galaxies are probably a scaled down version of normal spirals as far as their radio-continuum properties are concerned. Chyzy etal (1997) used the VLA to obtain power and polarization maps of two dIs (NGC4449 and IC10) and they were able to probe the existence of large scale magnetic field patterns, although of uncertain strength. Theoretically, one would expect magnetic fields of lower strength in dwarfs galaxies than in spirals as dynamo amplification ought to be less efficient due to the lower rotation speeds. Thus, a factor of 4 lower magnetic pressure in dwarfs, as required by the best fit to the velocity dispersion-metallicity data, is certainly reasonable and suggested by observations, although additional intense experimental efforts will be necessary in the future.

The oxygen yield from massive stars must still be considered as uncertain in spite of a number of recent detailed studies (Arnett 1978, Woosley & Weaver 1986, Thielemann *et al.* 1992, Maeder 1992). A nice comparison among the predictions of different theoretical models concerning this quantity can be found in Wang & Silk 1993 (see Fig. 1 of their paper). All models are in satisfactory agreement on the yields from stars with masses $\lesssim 30 M_\odot$, but they differ by up to a factor ≈ 10 for stars as massive as 80 $M_\odot$, depending on the metallicity. This difference, as already pointed out above, is due to the poorly known mass loss rate dependence on metallicity for massive stars and to the possible formation of a black hole. Fortunately, this variability range is much narrower when integration over a reasonable IMF is performed, due to the

rapid decrease of the number of very massive stars. Nevertheless, the adopted Maeder yields depend on metallicity and a comparison of our results with the ones obtained using the older Arnett prescriptions still produces a discrepancy of about 30% in the final oxygen abundance of the galaxy. This should be kept in mind when interpreting the comparison of our models with the data.

In addition to the uncertainties outlined, either caused by a experimental difficulties and/or by a limited theoretical understanding of various processes, there are obvious limitations and shortcomings of the present model. Maybe the most evident one is the lack of an attempt to model the possible occurrence of enhanced star formation periods (*i.e.,* starburst) during the evolution of the dI galaxies studied here. The motivation for this choice is twofold. Theoretically, the origin and characteristics of starbursts phenomena are not well understood: a large number of studies have tried to model these phenomena with limited success; it is beyond the frame of this work to review them properly. Observationally, there is no clear evidence that the majority of dIs go through starburst phases and that starbursts produce relevant evolutionary effects in addition to the ones produced by the underlying more quiescent star formation activity. The issue is nicely reviewed by Meurer (1999) who pointed out that the observed central surface brightness of bursting dIs is well below the one measured in BCDs: this indicates that dI starbursts are not even intense enough to be recognized as starbursts in many cases. In addition, a considerable fraction of BCDs (about 20%) shows no structural evidence (*i.e.,* they have nearly exponential μ and flat color profiles) for starbursts. Finally, as we have pointed out repeatedly here and in MF, the fractional ISM loss is modest even in starbursting prototypes as NGG1705 (Meurer *et al.* 1992). These remarks suggest that neglecting the role of starbursts is not seriously affecting the results presented here for dwarf galaxies, as also witnessed by the correct reproduction of the metallicity range observed for these objects.

Outflows rates of the order predicted here ($10^{-4} - 10^{-3} M_{\odot}$ yr^{-1}) may be traced and studied by X-ray and optical emission-line studies. Detailed numerical simulations by MF have shown that gaseous halos with sizes of tens of kpc are produced, with regions of high X-ray emissivity close to the galactic disk. Relatively cool, dense filaments also occur near the galaxy, well within the external shock, due to shell fragmentation, which are detectable by high spatial resolution experiments. In fact, the bulk of the observed X-ray emission may come from conductive interfaces associated with these structures, in which the emission is particularly enhanced by nonequilibrium effects. Detection via absorption line studies towards background objects such as QSOs has been also demonstrated (Bowen *et al.* 1997). Of course this type of experiment is limited by the low column densities in a large, rarefied halo, as well as the availability of suitably located, sufficiently bright, background objects, which are scarce for small dwarf galaxies. If these difficulties can be overcome,

this technique might provide unique information about the physical conditions prevailing in the outflows, and more generally, in dwarf halos.

6.1. A possible scenario

The results obtained in this study, together with previous theoretical and observational work, allow us to sketch a global evolutionary scenario for dwarf galaxies.

According to standard hierarchical models of structure formation, the star formation activity in the universe started with the formation of the so-called Pop III objects (Couchman & Rees 1986, Ciardi & Ferrara 1997, Haiman *et al.* 1997, Tegmark *et al.* 1997, Ferrara 1998, Ciardi, Ferrara & Abel 1999) at redshift $z \approx 30$. These are small (total mass $M \approx 10^6 M_\odot$ or baryonic mass $M_b \approx 10^5 M_\odot$) objects characterized by virial temperatures, T_{vir}, below the critical one ($T_H \approx 10^4$ K) at which the cooling necessary for the collapse cannot be provided by hydrogen lines (mostly Lyα line radiation), and molecular hydrogen is then, in a primordial plasma, the only efficient cooling agent. Translating the critical virial temperature into a total mass we obtain $M_H(z) = 4.4 \times 10^9 (1+z)^{-3/2} h^{-1} M_\odot$, where z is the virialization redshift. In order for collapse to take place it is required that the cooling time (whatever species is providing it) is shorter than the Hubble time at the epoch of virialization. This defines a second critical mass, $M_{crit}(z) < M_H$, which has been calculated by Tegmark *et al.* (1997). As a results only objects more massive than M_{crit} can indeed collapse and form luminous objects. The situation is somewhat complicated by feedback effects, involving the photodissociation of molecular hydrogen in Pop IIIs due to radiation, possibly created by neighbor sources. This prevents a fraction of objects, in spite of their mass being larger than M_{crit}, from collapsing. The strength of the feedback depends very much on the intensity of the radiation field and this involves detailed modelling out of the scope of this paper (these calculations are presented in Ciardi *et al.* 1999); neglecting this complication is not crucial for the argument we make here. The redshift evolution of both M_H and M_{crit} are shown in Fig. 12.

We can now compare these two masses with the ones derived for local dwarfs. The total masses of the best studied dSphs (Mateo *et al.* 1993 present the cases for 9 Local Group dSphs) range from $M_{tot} = 1.1 \times 10^7 M_\odot$ (Carina) up to $M_{tot} = 1.1 \times 10^9 M_\odot$ (NGC205). According to the previous definition $T_{vir} < T_H$, some of them can be classified as Pop IIIs, whereas the more massive ones probably belong to the class of objects able to cool via Lyα. Clearly, as M_H is redshift dependent, the classification depends on the formation epoch. The majority of Pop III objects can only live very short lifes due to their fragility,

and the dramatic feedback effects which can be induced by only a handful of SNe; their fate is inevitably a sudden death after the first star formation episode (which in most cases only involved the production of $< 1000 M_{\odot}$ of stars) and their leftover is a tiny naked stellar cluster without gas (but with DM), which could possibly be incorporated in larger structures. The ones which escape merging could still be seen in the nearby universe, although their expected extremely low luminosity should make their detection very challenging.

Is the absence of gas in these objects produced by blowaway in the early stages of their evolution ? The possibility that dEs are remnants of blown away PopIII objects has been proposed by Miralda-Escudé & Rees (1997). The results found here might suggest that this interpretation faces a mass discrepancy problem: we found that blowaway can occur only for total masses below $M_c \approx 5 \times 10^6 M_{\odot}$, which is several times smaller than the values derived by Mateo *et al.* for dSphs. One has to keep in mind that this value has been derived by assuming galaxy properties derived from observations of present day dwarfs and it implies that gaseous dwarfs, like dIs, with larger masses cannot transform into dEs *in the future*. However, the conditions at the formation, as the size, gas density, dark-to-visible mass ratio, of dwarfs' progenitors were probably very different. In particular, the critical mass for blowaway is extremely sensitive ($\propto \sigma^{10}$) to the level of turbulent motions in the ISM; finally, these quantities depend on the formation redshift and cosmological model. This discrepancy might be solved by putting the blowaway problem in a cosmological context. In fact, specific predictions for the Cold Dark Matter model with $\Omega_1, h = 0.5, \sigma_8 = 0.65$, have been made by Ciardi *et al.* (1999) who found that the critical mass for blowaway can be increased up to approximately 1-2 times M_H.

Although some uncertainty remains on the correct value of M_c as a result of the poorly known formation properties of galaxies, it is clear that blowaway is a very likely event in these small objects. This explanation is also favored by current galaxy formation scenarios. For example, Klypin *et al.* (1999) notice that most popular cosmological models would overpredict the number of low mass satellites in halos of galaxies like our own by a factor of about 4 with respect to what is observed. Theory can be brought in agreement with observations if it is assumed that these missing satellites are dark, *i.e.,* invisible due to their faintness as a result of gas ejection and quenching of star formation. Similar conclusions are reached also by Ciardi *et al.* (1999) who find that a consistent number of dark objects should be created as a byproduct of early galaxy formation. Additional support for the occurrence of blowaway has been brought by an interesting approach recently developed by Hirashita *et al.* (1998). These authors noted that a discontinuity is seen in the dependence of the virial mass/luminosity ratio (analogous to our ϕ parameter) on the virial

mass in a sample of local dSph at $M \approx 10^8 M_\odot$. They interpret this discontinuity as produced by blowaway, as low mass objects having lost most of their baryons would be characterized by high values of M_{vir}/L.

In addition to blowaway, other processes may be able to sweep away the galaxy ISM. Photoionization, either produced by external (Barkana & Loeb 1999) or internal (Lin & Murray 1992, Norman & Spaans 1997, Spaans & Norman 1998) sources, might have an important impact on the evolution of dwarfs. If a UV background (UVB), produced by QSOs and galaxies, is present it might even suppress the formation of dwarfs (Babul & Rees 1992, Efstathiou 1992, Thoul & Weinberg 1996, Nagashima *et al.* 1998). The common physical process on which these two ideas are based is that as the gas is photoionized, it is also heated to a temperature that exceeds the virial temperature of the halo itself and cannot be confined by the galaxy gravitational potential. The photoionization temperature of a moderately dense gas is, for a large range of properties of the radiation field and medium density, $T \approx 10^4$ K. Thus, the critical mass relative to photoionization effects essentially coincides with M_H: of course, this is not surprising as both temperatures are regulated by Lyα line cooling, which is an excellent thermostat.

Hence, dSphs must form before a consistent UVB is present in order to be able to accrete the gas, *i.e.,* before reionization; subsequently they can lose it when the UVB intensity has increased. In Fig. 12 the obliquely dashed region shows the mass-redshift parameter space were the formation of luminous objects regulated by the processes described above is allowed. The mass bounds of the shaded region are determined by the upper and lower mass limits of the 9 dSphs of the Mateo *et al.* (1993) sample, whose total mass values are superimposed (clearly, we do not know the virialization redshift of these objects). The first conclusion that we can draw from the Figure is that objects like Carina, Sculptor, Sextans, UMinor, and Draco are indeed Pop III objects which must have formed before $z \approx 15$ due to their low masses. Then at reionization, for which we have assumed the conservative lower redshift limit $z_i = 5$, they must have lost their gas either by photoevaporation or blowaway. An exception is represented by Sculptor in which a limited amount of HI ($M_{HI} \gtrsim 3 \times 10^4 M_\odot$) has been detected (Carignan *et al.* 1998). This gas is located at the edge of the galaxy optical image and its association with the galaxy is not completely clear. This gas could have been either part of a self-shielded and hence neutral intergalactic clump, or accreted recently thanks to the drop in the UV background, or IGM pressure confined ejected gas. Larger objects (Fornax, NGC147) could have formed at redshifts much closer that the reionization one and photoevaporated shortly after. NGC 185 and NGC 205 are instead consistently found to have some gas (Young & Lo 1997). This interpretation still has to face the question why dIs with total masses similar to dSphs (for a comparison see Tab. 1 and 2) yet are gas rich. If they have lost their gas in the past, they must have reaccreted material

relatively recently when the UVB intensity dropped. Environmental effects might play a role here, as we must require that dIs populate regions where gas accretion is more easily achieved than in those where dSphs of the same mass are found.

Whatever process (blowaway/photoionization) is setting the mass value M_c for gas ejection, might this fact be responsible for the separation between late type and early type dwarfs ? In other words, is it possible that these two galaxy types had common progenitors in the past but they evolved along different evolutionary paths determined by their mass and hence by their ability to retain their gas ? This is certainly an intriguing possibility which would solve the problems caused by a dI $\rightarrow$ dE transition occurring later on. If, as in the latter case, the transition has to be catalyzed by an intense stellar activity expelling the gas, then we should look at BCDs as objects on the point of being transformed into dEs. There are several, apparently insurmountable, difficulties associated with this interpretation, which can be briefly summarized as follows: although BCDs have clear similarities with dIs, however they have *(i)* higher surface brightness, *(ii)* larger radii with respect to dIs (Patterson & Thuan 1996); in addition, van Zee *et al.* (1997a,b) point out that BCDs have higher central mass concentration in both gas and stellar content. Even the second step of the dI $\rightarrow$ BCD $\rightarrow$ dE chain is problematic: the rotation curves of dIs are noticeably different from the ones of both dEs and BCDs, their kinematics being dominated by chaotic motions (Ferguson & Bingeli 1994). The alternative scenario proposed here, in which dI $\rightarrow$ dE transitions do not occur but these objects, starting from the same progenitors, have followed different evolutionary tracks, does not suffer from the above problems. In our view, BCDs would be simply represent a "normal" tail of the distribution of dwarfs massive enough to escape both blowaway/photoevaporation, in addition characterized by higher central mass density which favors the onset of occasional starbursts.

The consistency of our results for Leo A between effectively constant star formation rate over time and "bursty" behaviour shows that the properties of dI and BCD galaxies can be understood as fluctuations about a mean which is broadly constant/slowly decreasing, value with time. Bursts of star formation can happen easily in these small galaxies, but they do not last long enough to dramatically overwhelm the long term effects of low-level, but constant star formation, which is likely to represent the dominant mode of star formation (see also Tolstoy 1996, Cole *et al.* 1999, Gallagher *et al.* 1998). Intense bursts of star formation can make these small galaxies visible at cosmological distances, and their short duration can make the number density consistent with that of the faint blue galaxy population seen at intermediate redshifts (e.g. Tolstoy 1998a). The great diversity of properties of nearby dwarf galaxies (e.g. Mateo 1998, Toltoy 1998b) indicates that star formation rates can and do fluctuate noticeably on short timescales. It is also clear,

however, that there must be regulatory feedback processes, presumably like those presented here, which effectively average out these fluctuations over periods of several hundred million years. Although this is seemingly a long time on the timescale of an individual HII region, it is a more reasonable timescale for fluctations in the ISM and it is a negligible fraction of the lifetime of a galaxy.

7. Summary of the results

We have studied the role of stellar feedback produced by massive star formation and DM on the evolution of dwarf galaxies. The main results are the following:

• The entire gas content of a dwarf galaxy can be blown away if its total mass is $\lesssim 5 \times 10^6 M_\odot$; outflows occur in dwarfs with gas masses up to $\simeq 10^9 M_\odot$. Larger galaxies are not predicted to have a net mass loss, although a local circulation of gas via a fountain-type flow is possible. These conclusions closely agree with the results of MF.

• Even in the presence of an outflow, the predominant mechanism of gas consumption is the conversion of gas into stars. We conclude that outflows are affecting the properties of dwarfs only weakly.

• For a given visible galactic mass, the DM content correlates with the gas metallicity; from the available data we conclude that metallicities are consistent with a dark-to-visible mass ratio in dIs $\phi \simeq 0 - 30$. We predict the existence of a lower limit for the oxygen abundance in dIs 12+log(O/H) ≈ 7.2.

• Outflow rates from galaxies, when they occur, are in the range $10^{-5} - 0.04\ M_\odot\ \mathrm{yr}^{-1}$; The mass loss is a rather steep function of gas mass peaking at $M_g^f \approx$ few $\times\, 10^8 M_\odot$; these objects are therefore the major pollutants of the IGM.

• The HI velocity dispersion correlates with metallicity: independently of the DM content we predict that $\sigma \propto Z^{3.5}$. This relationship is found to agree nicely with the available data, particularly if about 1/4 of the ISM pressure is contributed by magnetic fields.

• We predict starf formation rates in the range $2 \times 10^{-3} - 0.07\ M_\odot\ \mathrm{yr}^{-1}$ for a galaxy with present day gas mass $M_g^f \approx 10^9 M_\odot$, depending on its DM content.

• For the specific case of the nearby dI Leo A, we forced the SFH of the galaxy to be the one experimentally derived from CMD studies; with this prescription our model correctly reproduces the observed metallicity of the galaxy. If the SFH is instead modelled as in the rest of the paper, the final

metallicity is equally well in agreement with the data.

• Based on our results, we discuss a scenario in which late type and early type dwarfs had common progenitors in the past, but the different total (mostly dark) mass produced a different evolution, governed by the combined effects of blowaway of the gas and photoionization. We consider dI → dE transitions (possibly through a BCD phase) occurring at present cosmic times as unlikely.

We would like to acknowledge useful discussions with B. Benjamin, D. Bowen, J. Dickey, D. Garnett, M.-M. Mac Low, M. Mateo, T. Thuan, and L. van Zee.

REFERENCES

Abbott, B. C., Bieging, J. H. & Churchwell, E. 1981, ApJ, 250, 645

Arnett, D. W. 1978, ApJ, 219, 1008

Arnett, D. W. 1990, in Chemical and Dynamical Evolution of Galaxies, eds. F. Ferrini *et al.* (Pisa: ETS), 409

Babul, A. & Rees, M. 1992, MNRAS, 253, 31

Babul, A. & Ferguson, H. C. 1996, ApJ, 458, 100

Barkana, R. & Loeb, A. 1999, preprint (astro-ph/9901114)

Binggeli, B. 1994, ESO/OHP Workshop on Dwarf Galaxies, eds. G. Meylan, P. Prugniel (ESO: Garching), 123

Binney, J. & de Vaucouleurs, G. 1981, MNRAS, 194, 679

Binney, J. & Tremaine, S. 1987, Galactic Dynamics (Princeton: UniPress)

Bomans, D. J., Chu, Y.-H., & Hopp, U. 1997, AJ, 113, 1678

Bowen, D. V., Tolstoy, E., Ferrara, A., Blades, J. C. & Brinks, E. 1997, ApJ, 478, 530

Broeils, A. H. & van Woerden, H. 1994, A&AS, 107, 129

Burkert, A. 1995 ApJ, 447, L25

Burkert, A., Theis, C. & Hensler, G. 1993 Dwarf Galaxies, ESO/OHP Workshop, eds. Meylan & Prugniel, 545

Carignan, C. 1998, in Dwarf Galaxies and Cosmology, eds. Thuan *et al.* , in press

Carignan, C., Beaulieu, S., Côté, S., Demers, S. & Mateo, M. 1998, AJ, 116, 1690

Casertano, S. P. R. & Shostak, G. S. 1980, A&A, 81, 371

Ciardi, B. & Ferrara, A. 1997, ApJL, 483, 5

Ciardi, B., Ferrara, A. & Abel, T. 1999, ApJ, in press

Ciardi, B., Ferrara, A., Governato, F. & Jenkins, A. 1999, in preparation

Cole A. A., Tolstoy E., Gallagher J. S., Hoessel J. G., Mould J. R., Holtzmann J. A., Saha A. & WFPC2 IDT 1999, AJ, in press

Couchman, H. M. P. & Rees, M. J. 1986, MNRAS, 221, 53

Chyzy, K., Urbanik, M., Kohle, S., Klein, U., Beck, R. & Berkhuijsen, E. M. 1997, in "Dwarf Galaxies: Probes for Galaxy Formation and Evolution", IAU JD

Clayton, D. D. & Pantelaki, I. 1993, Phys. Reports, 227, 293

Davies, J. & Phillips, S. 1988, MNRAS, 233, 553

Dekel, A. & Silk, J. 1986, ApJ, 303, 39

Della Ceca, R., Griffiths, R. E., Heckman, T. M. & Mackenty, J.W. 1996, ApJ, 469, 662

De Young, D. S. & Gallagher, J. S. III 1990, ApJ, 356L, 15

De Young, D. S. & Heckman, T. 1994, ApJ, 431, 598

Efsthatiou, G. 1992, MNRAS, 256, 43

Einasto, J., Saar, E., Kaasik, A. & Chernin, A. D. 1974, Nature, 252, 111

Ferguson, H. C. & Binggeli, B. 1994, A&AR, 6, 67

Ferrara, A. 1998, ApJ, 499, L17

Gallagher, J.S., Tolstoy, E., Saha, A., Hoessel, J., Dohm-Palmer, R.C., Skillman, E.D. & Mateo, M. 1998, AJ, 115, 1869.

Haiman, Z., Rees, M. J., & Loeb, A. 1997, ApJ, 484, 985

Han, M., Hoessel, J. G., Gallagher, J. S. III, Holtsman, J & Stetson, P. B. & WFPC2/IDT 1997, AJ, 113, 1001

Heckman, T. H., Dahlem, M., Lehnert, M. D., Fabbiano, G., Gilmore, D. & Waller, W. H. 1995, ApJ, 448, 98

Hirashita, H., Takeuchi, T. T. & Tamura, N. 1998, ApJL, 504, 83

Huchtmeier, W. K. & Richter, G. 1988, A&A, 203, 237

Hunter, D. A., Gallagher, J. S. & Rautenkranz, D. 1982, ApJS, 49, 53

Hunter, D. A., Wilcots, E. M., van Woerden, H., Gallagher, J. S., Kohle, S. 1998, ApJL, 495, 47

Klein, U., Giovanardi, C., Altschuler, D. R. & Wunderlich, E. 1992, A&A, 255, 49

Klein, U., Hummel, E., Bomans, D. J. & Hopp, U. 1996, A&A, 313, 396

Klypin, A. A., Kravtsov, A., Valenzuela, O. & Prada, F. 1999, ApJ, submitted (astro-ph/9901240)

Knapp, G. R., Kerr, F. J. & Bowers, P. F, 1978, AJ, 83, 360

Koeppen, J., Theis, C. & Hensler, G. 1995, A&A, 296, 99

Koo, B. C. & McKee 1992, ApJ, 388, 103

Kompaneets, A. S. 1960, Sov. Phys. Dokl., 5, 46

Larson, R. B. 1974, MNRAS, 166, 585

Lacey, C. & Silk, J. 1991, ApJ, 381, 14

Lequeux, J, Rayo, J. F., Serrano, A., Peimbert, M. & Torres- Peimbert, S. 1979, A&A, 80, 155

Lin, D. N. C. & Faber, S. M. 1983, ApJL, 266, 21

Lin, D. N. C. & Murray, S. D. 1992, ApJ, 394, 523

Lisenfeld, U. & Ferrara, A. 1998, ApJ, 496, 145

Lo, K. Y., Sargent, W. L. W., Young, K. 1993, AJ, 106, 507

Mac Low, M.-M., McCray, R. & Norman, M. L. 1989, ApJ, 337, 141

Mac Low, M.-M., & Ferrara, A. 1999, ApJ, in press (astro-ph/9801237) (MF)

Maeder A., 1992, A&A, 264, 105

Marconi, G., Matteucci, F. & Tosi, M. 1994, MNRAS, 270, 35

Mateo, M. 1988, ApJ, 331, 261

Mateo, M. 1993, in Dwarf Galaxies, ESO/OHP Workshop, eds. Meylan & Prugniel, 309

Mateo, M. 1998, ARA&A, 36, 435

Matteucci, F. & Chiosi, C. 1983, A&A, 123, 121

Matteucci, F. & Tosi, M. 1985, MNRAS, 217, 391

Meurer, G. R., Freeman, K. C., Dopita, M. A., Cacciari, C. 1992, AJ, 103, 60

Meurer, G. R. 1999, in Dwarf Galaxies and Cosmology, XIII Moriond Meeting, eds. T. X. Thuan etal., in press (astro-ph/9806304)

Miniati, F., Jones, T. W., Ferrara, A. & Ryu, D. 1997, ApJ, 491, 216

Miniati, F. Ryu, D., Ferrara, A. & Jones, T. W. 1999, ApJ, 510, 726

Minniti, D. & Zijlstra, A. 1996, ApJL, 467, 13

Miralda-Escude, J. & Rees, M. 1997, ApJ, 497, 21

Nagashima, M., Gouda, N. & Sugiura, N. 1998, MNRAS 301, 849

Norman, C. A., & Ferrara, A. 1996, ApJ, 467, 280

Norman, C. A., & Spaans, M. 1997, ApJ, 480, 145

Padoan, P., Nordlund, A., Jones, B. J. T. 1997, MNRAS, 288, 43

Pagel, B. E. J., Simonson, E. A., Terlevich, R. J. & Edmunds, M. G. 1992, MNRAS, 255, 325

Papaderos, P., Fricke, K. J., Thusn, T. X. & Loose, H. -H. 1994, A&A, 291, L13

Patterson, R. & Thuan, T. 1996, ApJSS, 107, 103

Persic, M., Salucci, P. & Stel, F. 1996, MNRAS, 281, 27P

Pryor, C. 1996, The Formation of the Galactic Halo: Inside and Out, ASP Conf. Ser., Vol. 92, eds. H. Morrison and A. Sarajedini, (San Francisco: PASP), 424

Puche, D., Westphal, D., Brinks, E. & Roy, J.-R. 1992, AJ, 103, 1841

Puche, D. & Westphal, D. 1993, in Dwarf Galaxies, ESO/OHP Workshop, eds. Meylan & Prugniel, 273

Richer, M. G., McCall, M. L. & Stasinka, G. 1999, A&A in press (astro-ph/9809302)

Ricotti, M., Ferrara, A. & Miniati, F. 1997, ApJ, 485, 254

Salpeter, E. E. & Hoffman, G. L. 1996, ApJ, 465, 595

Scalo, J. M. 1986, Fund. Cosm. Phys., 11, 1

Silk, J. 1997, ApJ, 481, 703

Skillman E. D., Melnick, J., Terlevich, R. & Moles, M. 1988, A&A, 196, 31

Skillman, E. D., Kennicutt, R.C. & Hodge, P. W. 1989, ApJ, 347, 875

Smecker-Hane, T. A., Stetson, P. B., Hesser, J. E. & Lehnert, M. D. 1994, AJ, 108, 507

Spaans, M. & Norman, C. A. 1997, ApJ, 483, 87

Spitzer, L. 1978, Physical Processes in the Interstellar Medium, (New York: Wiley)

Staveley-Smith, L., Davies, R. D. & Kinman, T. D. 1992, MNRAS, 258, 334

Suntzeff, N. B., Mateo, M., Terndrup, D. M., Olszewski, E. W., Geisler, D. & Weller, W. 1993, ApJ, 418, 208

Taylor, C. L. 1997, ApJ, 480, 524

Tegmark, M., Silk, J., Rees, M.J., Blanchard, A., Abel, T. & Palla, F. 1997, ApJ, 474, 1

Thielemann, F. K., Nomoto, K. & Hashimoto, M. 1992, Structure and Evolution of Neutron Stars, (Knudsen), 298

Thoul, A. & Weinberg, D. H. 1996, ApJ, 465, 608

Tinsley, B. M. 1980, Fund. Cosm. Phys., 5, 287

Tolstoy, E. 1996, ApJ, 462, 684

Tolstoy, E. & Saha, A. 1996, ApJ, 462, 672

Tolstoy, E., Gallagher, J.S., Saha, A., Hoessel, J., Skillman, E.D., Dohm-Palmer, R.C., Mateo, M. & Hurley-Keller D. 1998, AJ, 116, 1244

Tolstoy, E. 1998a, in Dwarf Galaxies and Cosmology, eds. Thuan *et al.* , in press (astro-ph/9807154)

Tolstoy, E. 1998b, in The Stellar Content of Local Group Galaxies, eds. Whitelock & Cannon, in press (astro-ph/9901245)

Vader, J. P. 1986, ApJ, 305, 669

Vader, J. P. 1987, ApJ, 317, 128

van Zee, L., Haynes, M. P. & Salzer, J. J. 1997a, AJ, 114, 2479

van Zee, L., Haynes, M. P. & Salzer, J. J. 1997b, AJ, 114, 2497

van Zee, L., Haynes, M. P., Salzer, J. J., & Broeils, A. 1997, AJ, 113, 1618

van Zee, L., Maddalena R. J., Haynes, M. P., Hogg, D. E. & Roberts, M. S. 1997, AJ, 113, 1638

van Zee, L., Skillman, E.D. & Salzer, J. J. 1998, AJ, 116, 1186

Wang, B. & Silk, J. 1993, ApJ, 406, 580

Wilcots, E.M. & Miller B.W. 1998, AJ, 116, 2363

Wyse, R. F. G. & Silk, J. 1985, ApJL, 269, 1

Woosley, S. E. & Weaver, T. A. 1986, ARA&A, 24, 205

Young, L. M. & Lo, K. Y. 1996, ApJ, 462, 203

Young, L. M. & Lo, K. Y. 1997a, ApJ, 476, 127

This manuscript was prepared with the AAS LaTeX macros v4.0.

Table 1: Sample Dwarf Galaxy Properties

Galaxy	Z[a]	M_{HI}[b]	M_{tot}[b]	ϖ_*[b]	Σ_B[c]	σ_{ISM}[c]
	12+log(O/H)	$10^7 M_\odot$	$10^7 M_\odot$	kpc	$L_\odot pc^{-2}$	km s^{-1}
NGC2366	7.96	74.13	180	7.73	45.9	-
NGC1569	8.16	11.22	50	3.94	317.4	-
NGC4214	8.34	112.20	320	12.47	0.87	-
NGC4449	8.32	154.88	620	8.06	200.3	-
UGC4483	7.32	5.01	10	1.21	18.3	-
DDO167	7.66	1.26	7	1.92	22.	-
DDO187	7.36	2.04	10	1.76	20.	-
DDO47	7.85	6.03	140	5.20	7.3	-
SMC†	7.98	48.98	50	4.93	66.3	-
SagDIG†	7.42 ± 0.3	0.88± 0.19	0.96	0.83	11.52[e]	7.5 ± 2
GR 8†	7.62 ± 0.1	0.45± 0.14	6.0	0.96	79.73[e]	11 ± 3
Leo A†	7.30 ± 0.1	8.0 ± 0.8	6.0	0.98	15.2	9.3*/3.5*
WLM†	7.75 ± 0.2	6.1 ± 0.6	40	2.75	476.0[e]	8
IC5152†	8.36 ± 0.2	5.9 ± 1.1	30	1.95	50.3	8
IC1613†	7.8 ± 0.2	5.4 ± 1.1	79.5	2.94	50.31[e]	8.5* ± 1
Sex A†	7.49 ± 0.2	7.8 ± 1.3	39.5	3.12	26.4[e]	8 ± 3
Sex B†	7.84 ± 0.3	4.5 ± 0.6	30.	3.49	34.8	18
NGC6822†	8.2 ± 0.2	13.4± 1.8	164	2.02	182.6[e]	8
IC10†	8.19 ± 0.15	15.3± 3.5	158	1.94	95.86[e]	8* ± 2
PegDig†	7.93 ± 0.14	5.4 ± 0.6	5.8	0.62	26.4	8.6* ± 1.4
NGC 55†	8.32 ± 9.15	139 ± 22.4	1560	14.12	317.4[e]	8
NGC3109†	8.06 ± 0.2	69 ± 14	655	7.56	23.91[e]	10 ± 2

[a] from Skillman *et al.* 1989 or Mateo 1998; error estimates from Mateo 1998

[b] from Huchtmeier and Richter 1988; or Mateo 1998

[c] from Mateo 1998 or RC3

† Local Group galaxy (most numbers come from Mateo 1998)

Table 2: The Van Zee Sample

Galaxy	Z[a]	M_{HI}[b]	M_{tot}[b]	ϖ_*[b]	$<\Sigma_B>_{25}$[b]	σ_{ism}[b]
	12+log(O/H)	$\times 10^7 M_\odot$	$\times 10^7 M_\odot$	kpc	$L\odot pc^{-2}$	km s^{-1}
UGC 300	7.8±0.1	93*	-	-	-	-
UGC 521	7.9±0.1	95*	407*	-	-	-
UGCA 20	7.6±0.1	25	506	8.66	4.18	9.0
UGC 2684	7.6±0.1	15	157	4.51	7.97	7.6
UGC 2984	8.3±0.2	692*	-	-	20.0	-
UGC 3174	7.8±0.1	61	911	9.34	31.7	9.2
UGC 5716	8.1±0.1	140	1820	13.67	20.0	9.5
UGC 7178	-	140	1720	12.71	13.9	8.0
UGC 11820	8.0±0.2	440	3910	21.21	22.0	8.6
UGC 191	8.12[c]±0.03	320	3250	15.97	55.2	11.2
UGC 634	8.18[c]±0.03	470	6770	19.90	31.7	11.4
UGC 891	8.20[c]±0.10	100	1080	11.48	24.1	8.8
UGC 5764	7.92[c]±0.03	34	303	6.60	45.9	9.7
UGC 5829	8.28[c]±0.10	182*	2188*	-	-	-
UGC 8024	7.67[c]±0.06	12*	220◇	6◇	-	-
UGC 9128†	7.75[c]±0.05	3.5*	10◇	1.76◇	-	-
UGC 3672	8.0± 0.1	129*	355*	-	-	-
UGCA 357	8.05±0.05	191*	501*	-	-	-
Haro 43	8.20±0.1	229*	295*	-	-	-

[a] from van Zee, Haynes & Salzer (1997a)

[b] from van Zee, Haynes, Salzer & Broeils (1997)

[c] from van Zee, Haynes & Salzer (1997b)

* from van Zee, Maddalena, Haynes, Hogg & Roberts (1997)

◇ from Huchtmeier & Richter 1988

† DDO187

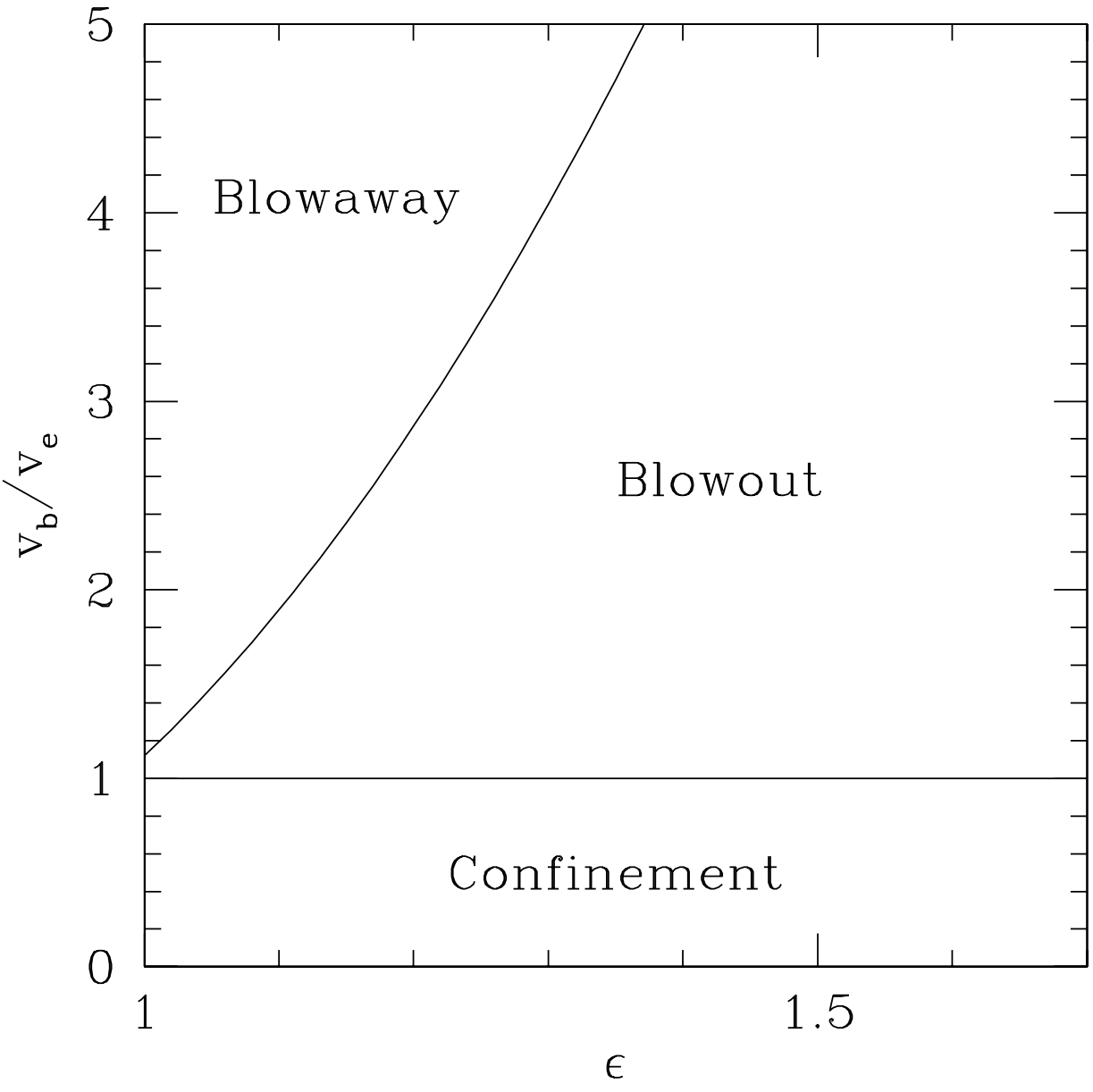

Fig. 1.— Conditions for blowaway, blowout and confinement as a function of the major-to-minor axis ratio $\epsilon = \varpi_*/H$ of dwarfs galaxies; $\epsilon = 1$ corresponds to spherical bodies.

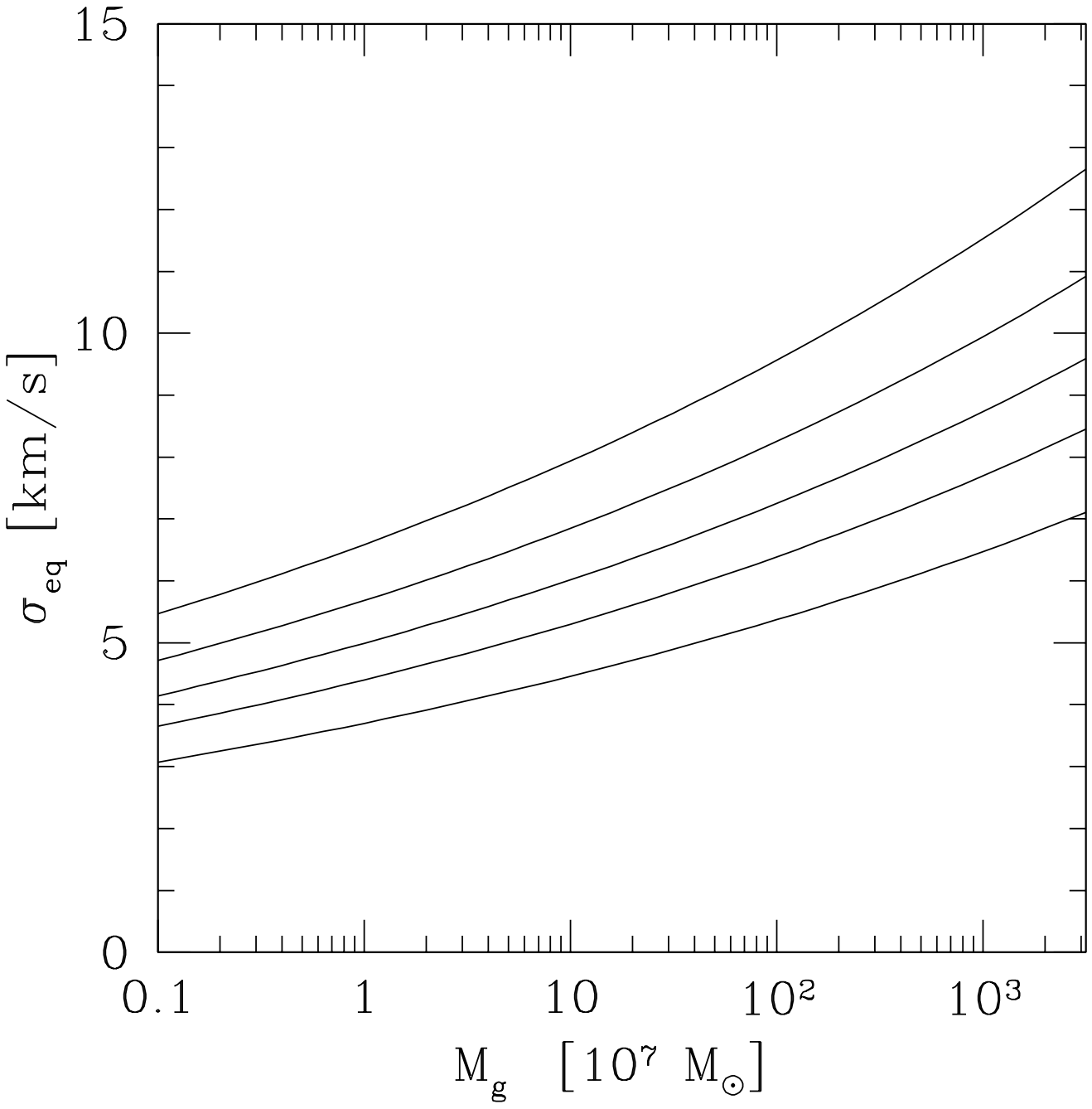

Fig. 2.— Velocity dispersion equilibrium value, σ_{eq}, as a function of galactic gas mass and for different values of $\phi = 0, 3, 10, 30, 100$ from the lowermost to uppermost curve, respectively.

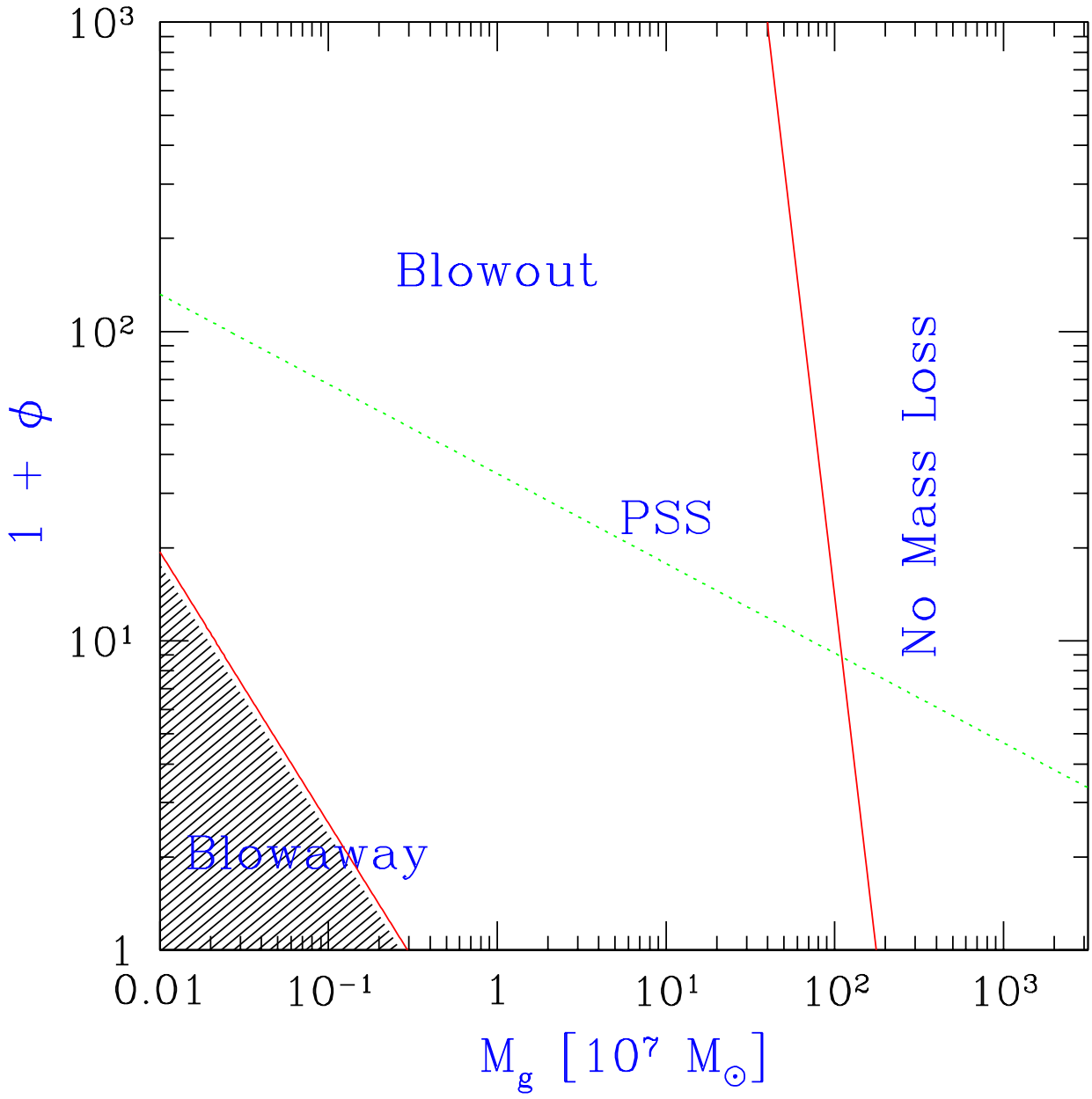

Fig. 3.— Regions in the $\phi - M_g$ plane in which different dynamical phenomena (see text for definitions) may occur, explicitly derived in eqs. 53-52. Also shown is the locus of points describing the Persic *et al.* (PSS) $\phi - M_g$ relation (dotted line).

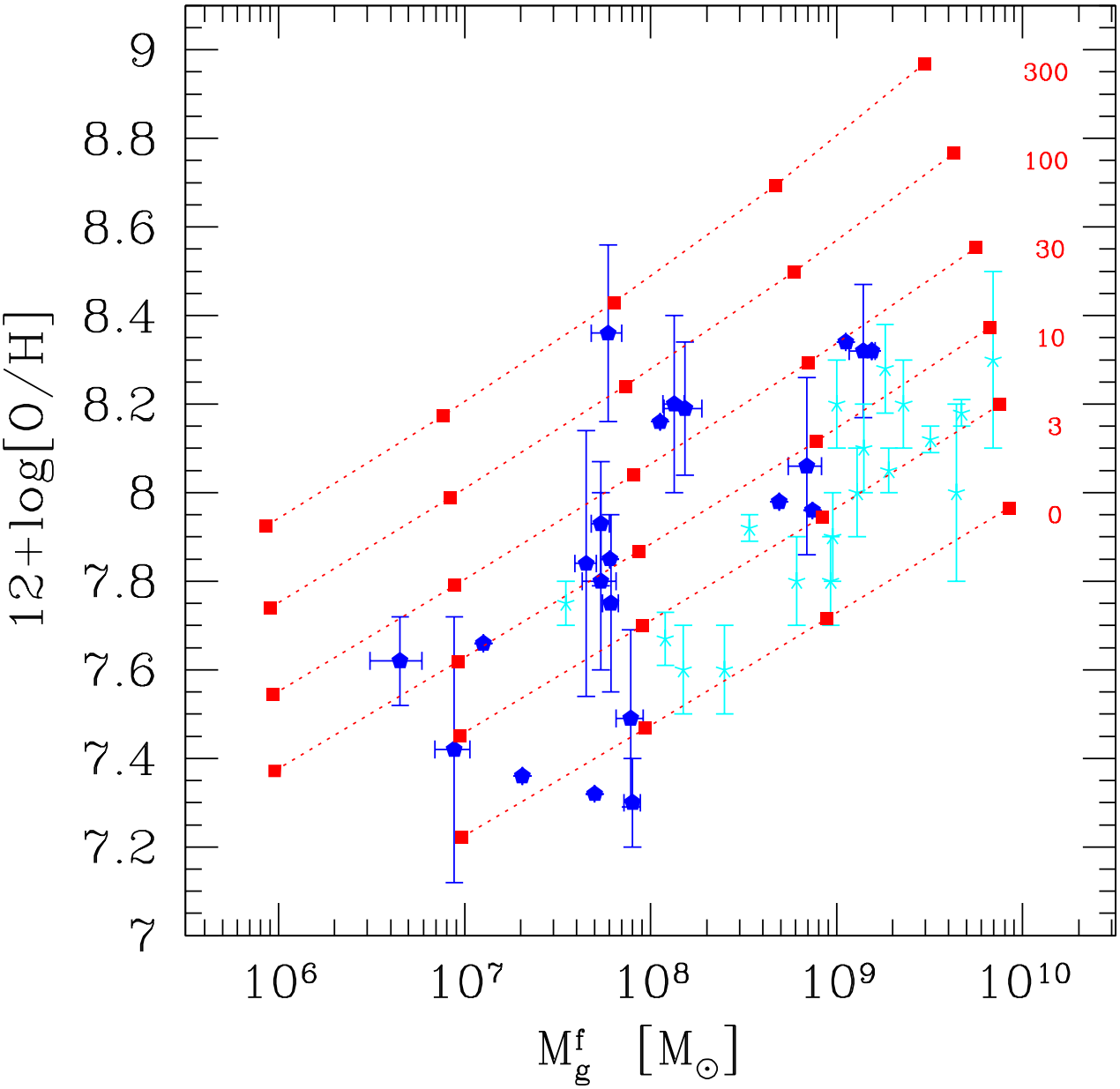

Fig. 4.— Model results for the oxygen abundance as a function of the final gas mass M_g^f for different values of $\phi = 0, 3, 10, 30, 100, 300$ (squares); points show the data from the Skillman (pentagons) and van Zee (stars) samples.

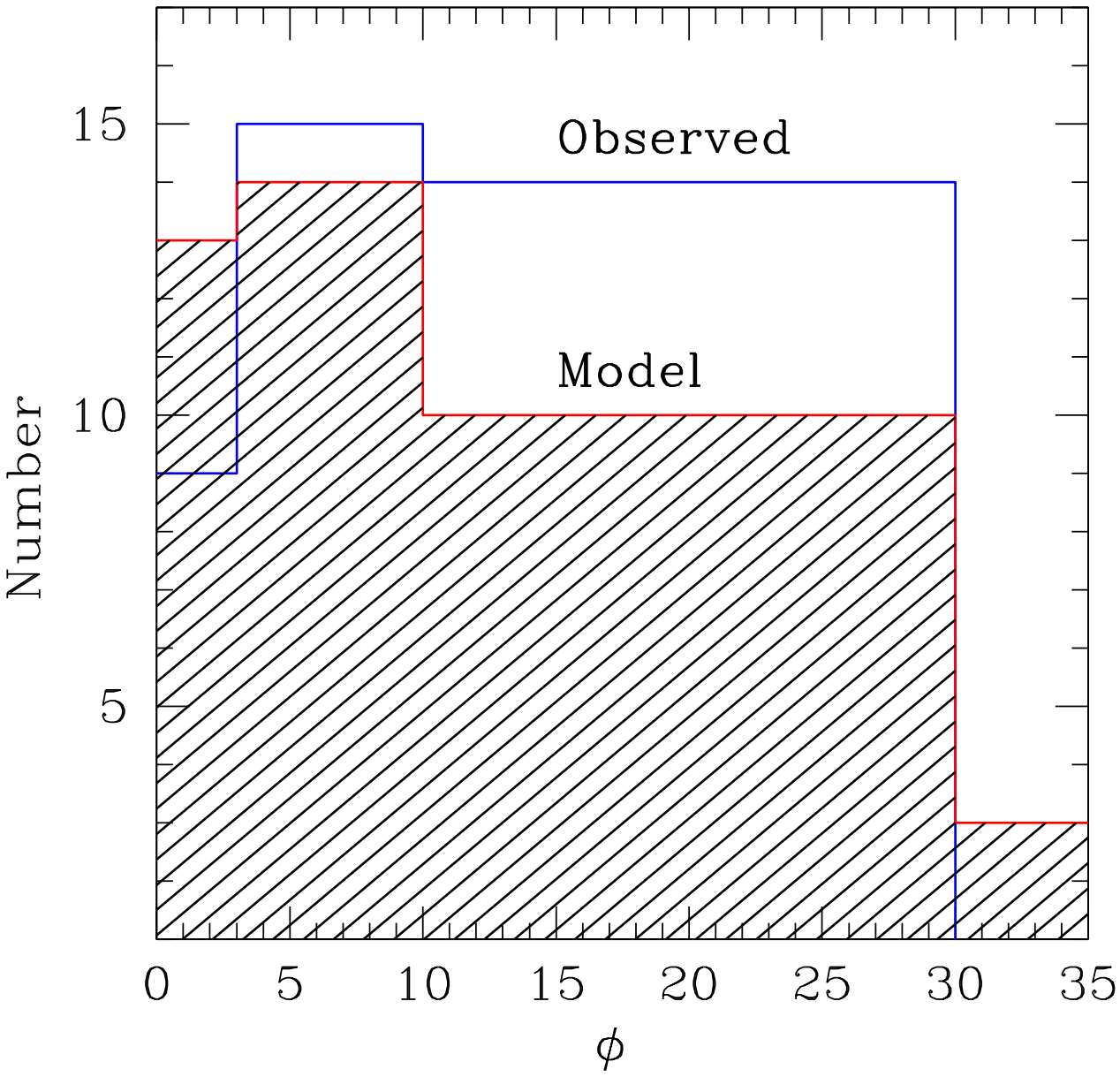

Fig. 5.— Distribution of the observationally inferred dark-to-visible ratio, ϕ, for the galaxy compared with the one derived from the model.

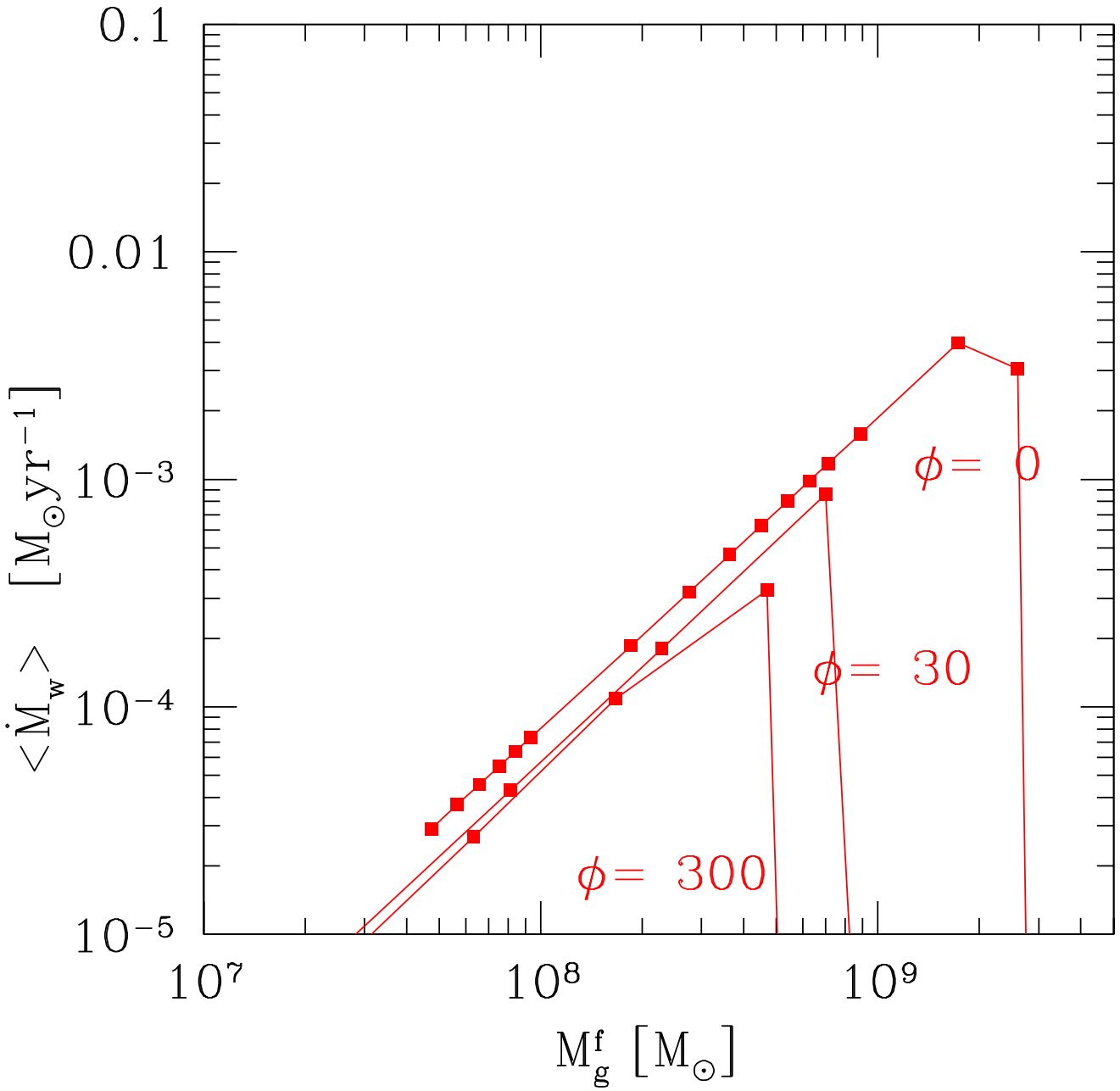

Fig. 6.— Time-averaged mass outflow rate $\langle \dot{M}_w \rangle$ as a function of the final gas mass M_g^f for three different values of $\phi = 0, 30, 300$.

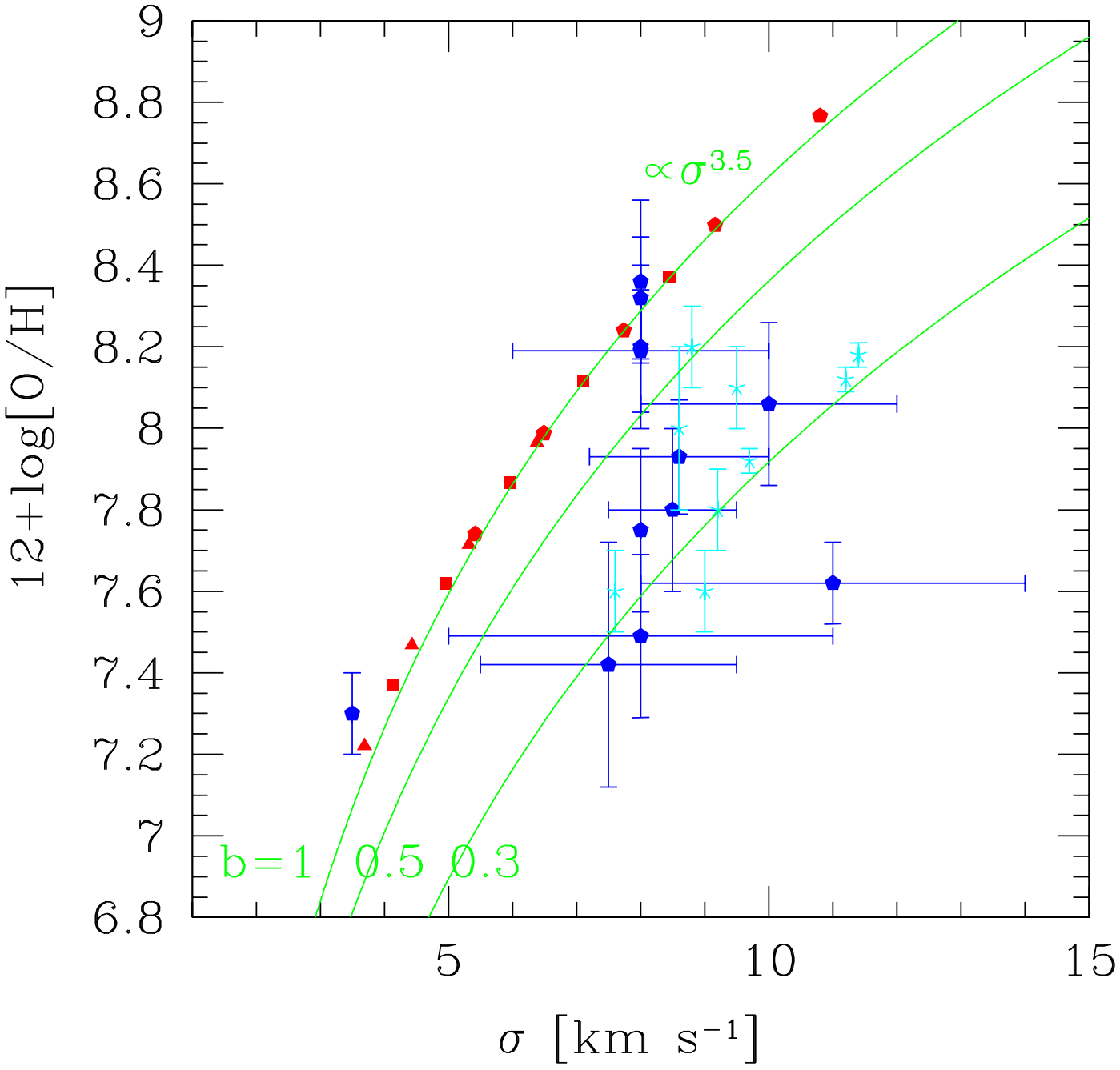

Fig. 7.— Relation between oxygen abundance and gas velocity dispersion for $\phi = 0$ (triangles),$\phi = 10$ (squares), $\phi = 100$ (pentagons). A fit to the relation is also shown for three values of the magnetic reduction factor $b_1 = 1.0, 0.5, 0.3$ (solid lines). Data points are from the Skillman (pentagons) and Van Zee (stars) sample.

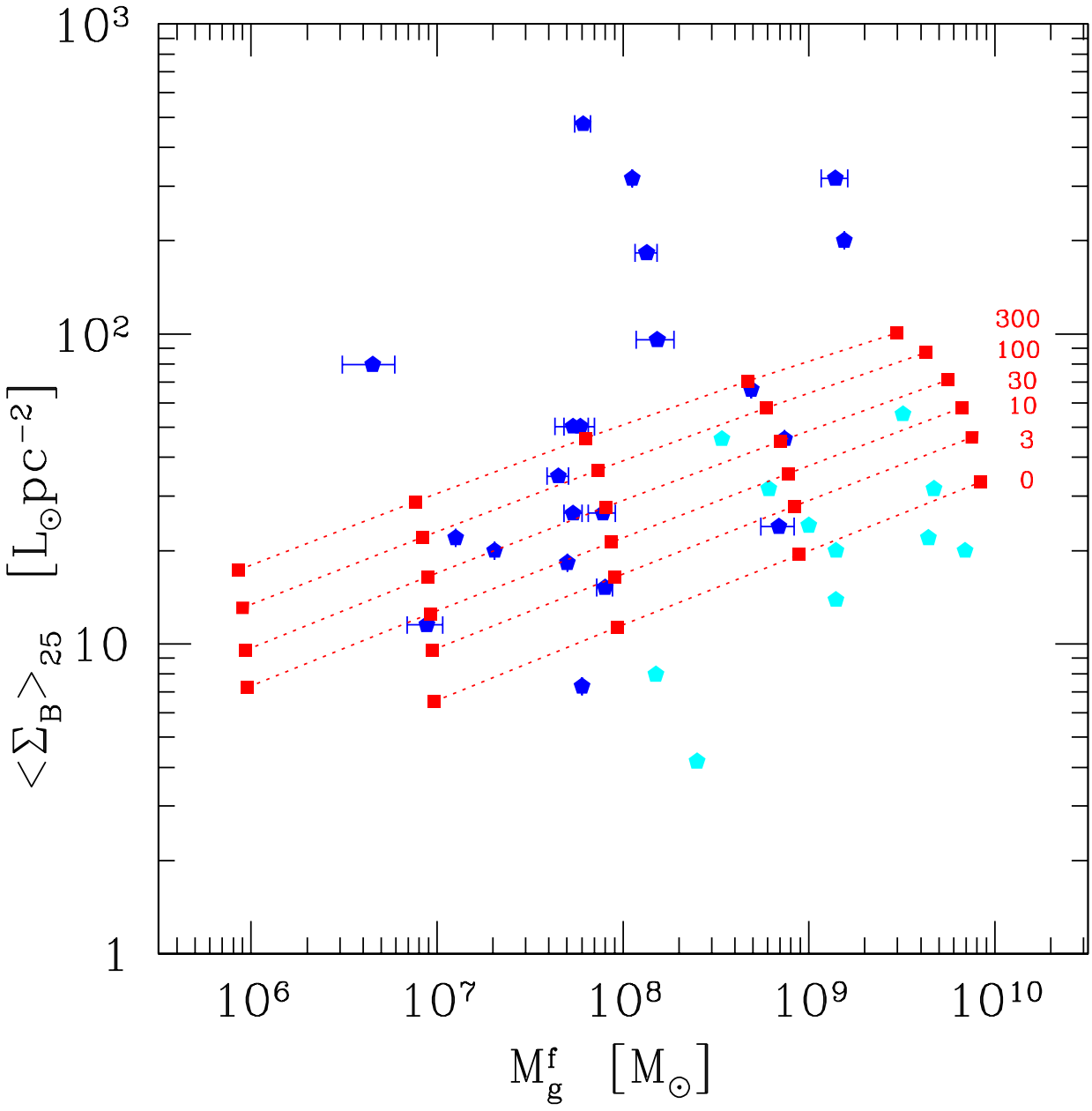

Fig. 8.— Surface brightness at B=25 as a function of the final gas mass M_g^f for different values of $\phi = 0, 3, 10, 30, 100, 300$ (squares); pentagons show the data from the Skillman sample.

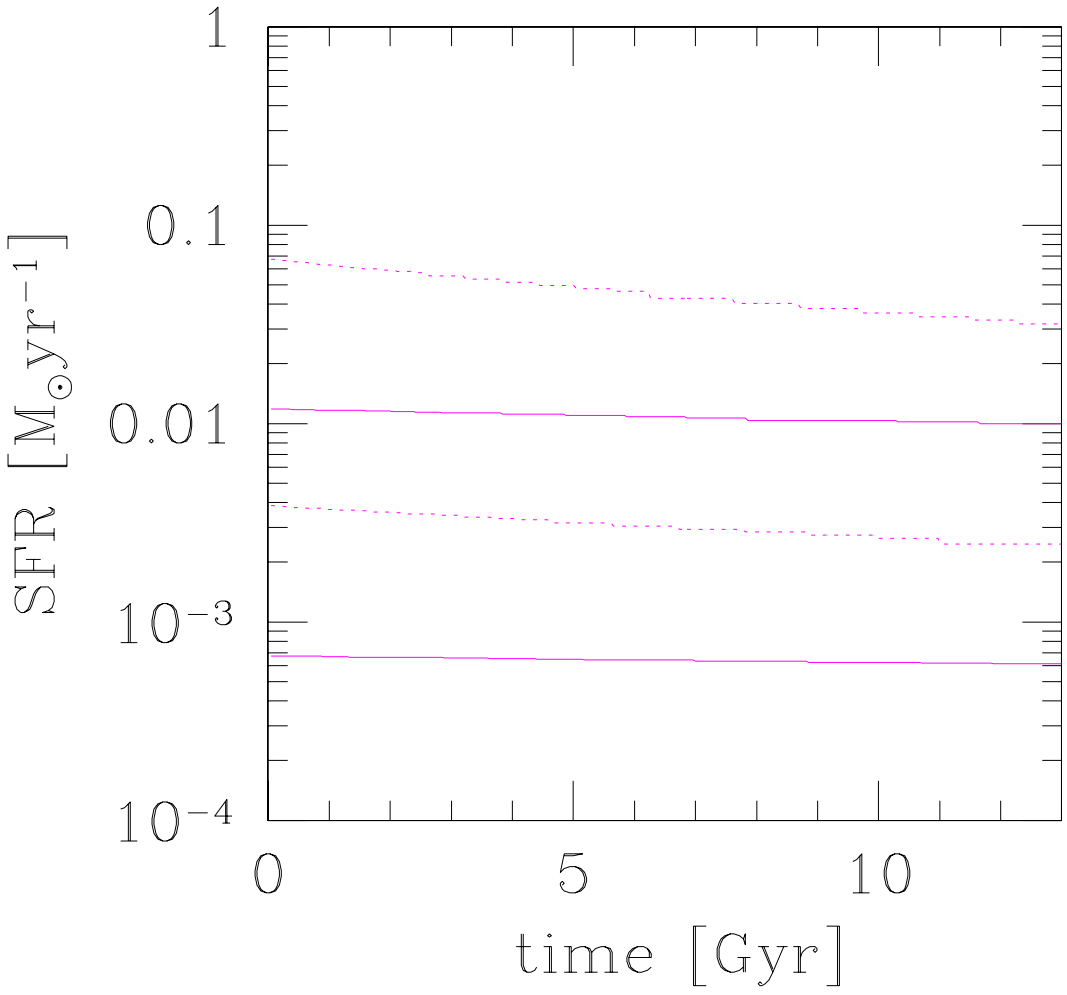

Fig. 9.— Evolution of the star formation rate for four different galaxies with final gas masses $M_g^f \approx 10^8 M_\odot$ (solid curves) and $M_g^f \approx 10^9 M_\odot$ (dotted); for each mass two values of $\phi = 0$ (lowermost) and $\phi = 30$ (uppermost) are shown.

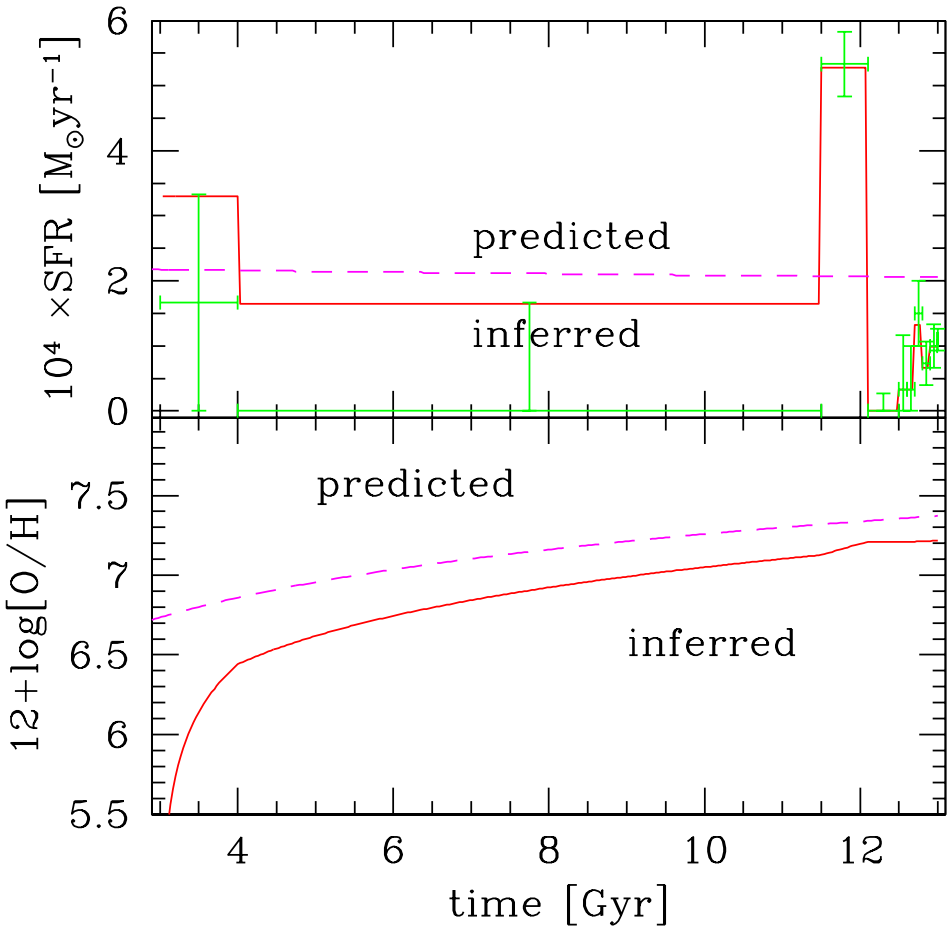

Fig. 10.— *Upper panel*: star formation history for the galaxy Leo A inferred from CMD diagrams compared with the one predicted from the model; *Lower panel*: evolution of metallicity for the two SFHs. Both give final oxygen abundances within the errors of the currently observed value $12 + \log[O/H] = 7.3 \pm 0.1$.

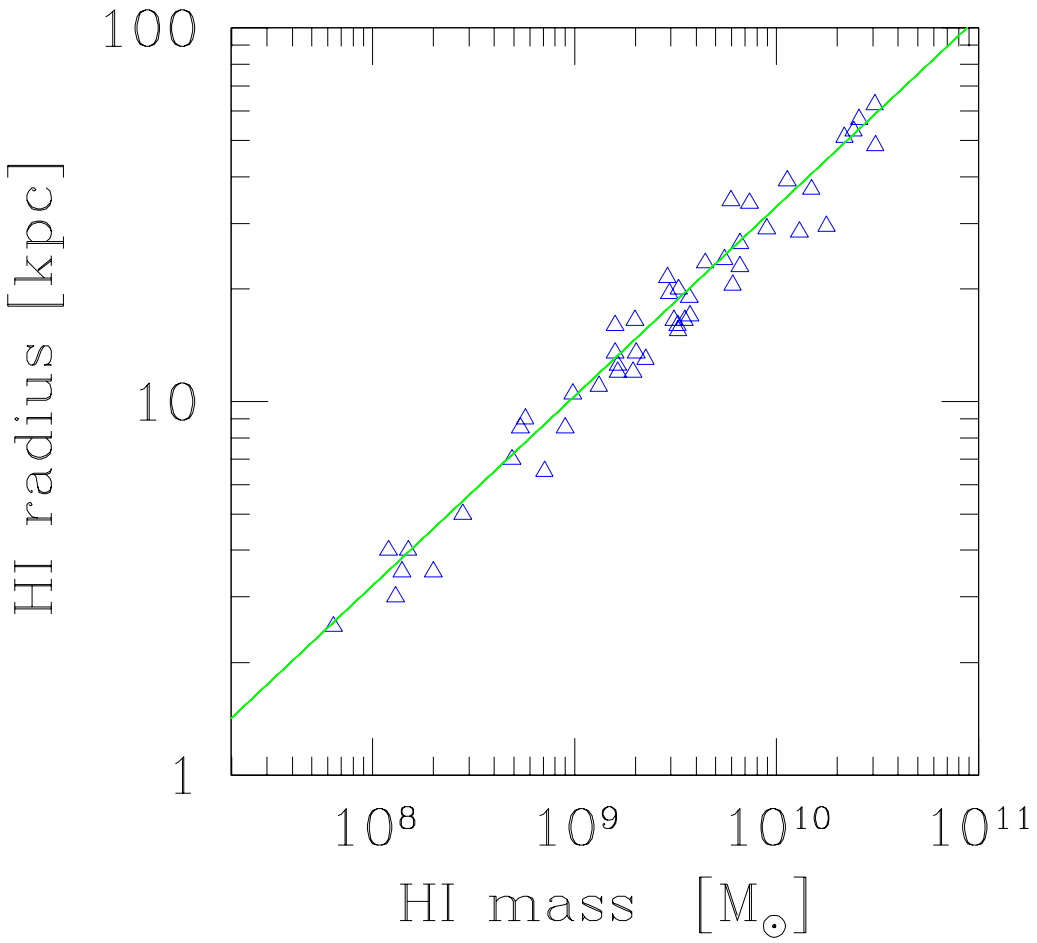

Fig. 11.— Comparison between the analytical HI radius-mass relation adopted in this work eq. 13 (solid line) and the data from Broeils & van Woerden 1994 (triangles). The line is *not* a fit to the data.

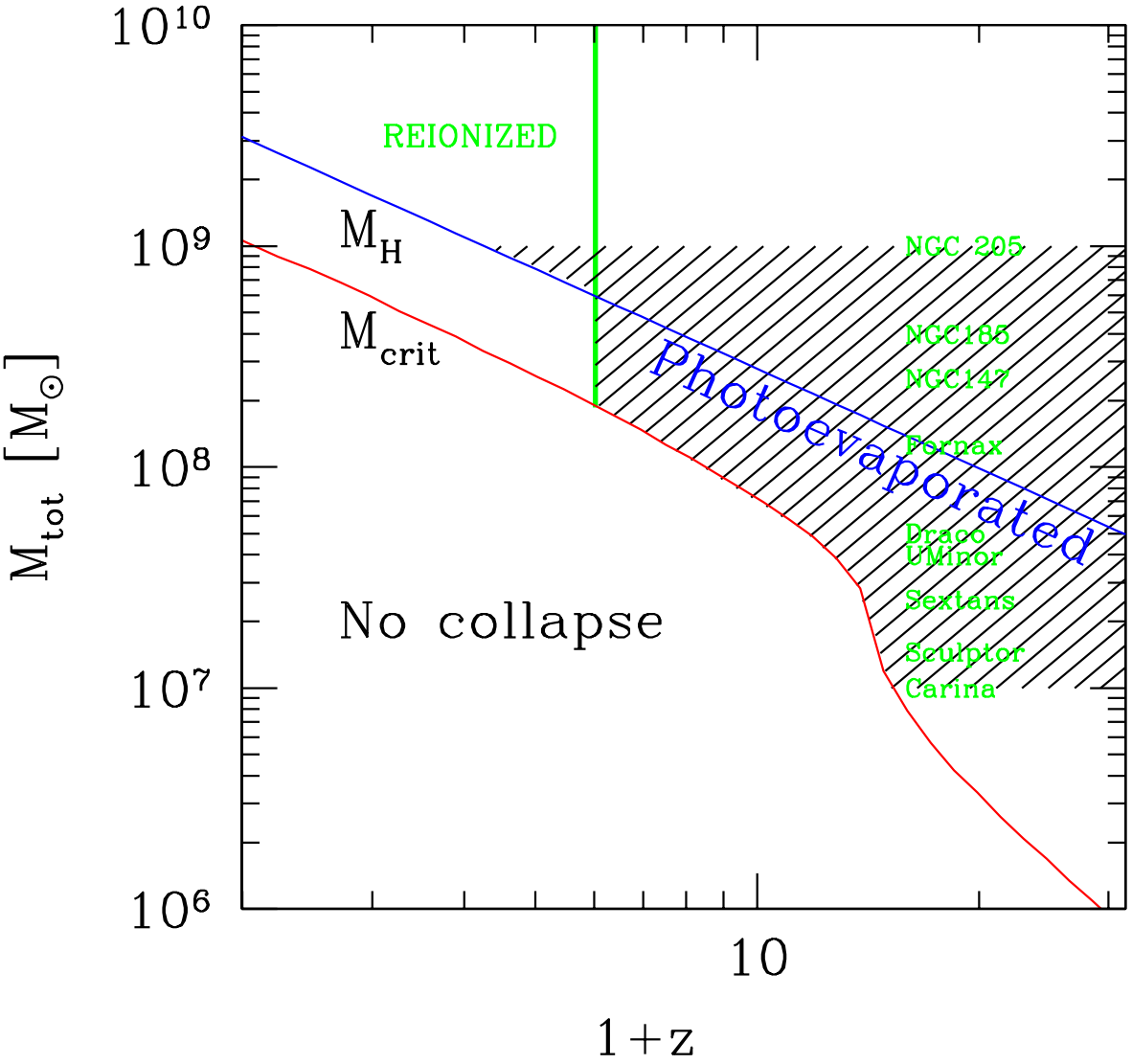

Fig. 12.— Redshift evolution of the critical mass for collapse, M_{crit}, and for photoevaporation, M_H. The dashed region corresponds to the mass-formation redshift space of objects with total masses in the range of LG dSphs, whose names are listed. Objects with $M < M_H$ can form but they are photoevaporated at reionization (vertical line) or blown away; objects with $M > M_H$ can form even after reionization and survive photoevaporation.